Development 140, 1550-1559 (2013) doi:10.1242/dev.087130

Lethal giant larvae 2 regulates development of the ciliated organ Kupffer's vesicle

Hwee Goon Tay[1], Sabrina K. Schulze[2], Julien Compagnon[3], Fiona C. Foley[1], Carl-Philipp Heisenberg[3], H. Joseph Yost[4], Salim Abdelilah-Seyfried[2] and Jeffrey D. Amack[1]*

SUMMARY

Motile cilia perform crucial functions during embryonic development and throughout adult life. Development of organs containing motile cilia involves regulation of cilia formation (ciliogenesis) and formation of a luminal space (lumenogenesis) in which cilia generate fluid flows. Control of ciliogenesis and lumenogenesis is not yet fully understood, and it remains unclear whether these processes are coupled. In the zebrafish embryo, *lethal giant larvae 2* (*lgl2*) is expressed prominently in ciliated organs. Lgl proteins are involved in establishing cell polarity and have been implicated in vesicle trafficking. Here, we identified a role for Lgl2 in development of ciliated epithelia in Kupffer's vesicle, which directs left-right asymmetry of the embryo; the otic vesicles, which give rise to the inner ear; and the pronephric ducts of the kidney. Using Kupffer's vesicle as a model ciliated organ, we found that depletion of Lgl2 disrupted lumen formation and reduced cilia number and length. Immunofluorescence and time-lapse imaging of Kupffer's vesicle morphogenesis in Lgl2-deficient embryos suggested cell adhesion defects and revealed loss of the adherens junction component E-cadherin at lateral membranes. Genetic interaction experiments indicate that Lgl2 interacts with Rab11a to regulate E-cadherin and mediate lumen formation that is uncoupled from cilia formation. These results uncover new roles and interactions for Lgl2 that are crucial for both lumenogenesis and ciliogenesis and indicate that these processes are genetically separable in zebrafish.

KEY WORDS: Cilia, Lumenogenesis, Lethal giant larvae 2, Rab11a, Left-right asymmetry, Zebrafish

INTRODUCTION

In several organs, motile cilia extending from epithelial cells beat in a coordinated fashion to move fluids. Disruption of proteins that regulate cilia function can result in a broad spectrum of clinical disorders known as ciliopathies (Sharma et al., 2008). In the zebrafish embryo, Kupffer's vesicle, otic vesicles and the pronephric ducts are examples of organs that assemble motile cilia that project into a lumen and generate fluid flow that is necessary for normal development (Essner et al., 2005; Kramer-Zucker et al., 2005; Yu et al., 2011). In ciliated organs, formation and maintenance of cilia requires docking of a basal body to the apical cell surface, vesicle trafficking of ciliary proteins from the Golgi apparatus to the cilium and movement of cargos through the cilia via intraflagellar transport (Ishikawa and Marshall, 2011). At the same time, formation of a lumen requires specific modification of the cytoskeleton, polarized vesicle trafficking to the lumenal surface and regulation of cell junctions (Rodríguez-Fraticelli et al., 2011). Our understanding of how ciliogenesis and lumenogenesis are regulated as individual processes remains incomplete, but even less is known about the relationship between these two processes. Here, we show that zebrafish Lethal giant larvae 2 (Lgl2; Llgl2 – Zebrafish Information Network) is a regulator of both lumenogenesis and ciliogenesis and that these processes can be uncoupled in developing ciliated organs.

First identified as a tumor suppressor in *Drosophila* (Gateff, 1978), Lgl proteins regulate several cellular activities, including apicobasal polarization, asymmetric division, and migration (Atwood and Prehoda, 2009; Betschinger et al., 2003; Kaplan et al., 2009; Tanentzapf and Tepass, 2003). In epithelial cells, Lgl interacts antagonistically with atypical protein kinase C (aPKC) to establish basolateral membrane domains and to position cell junctions (Betschinger et al., 2005; Plant et al., 2003). Lgl may target proteins to specific membrane locations by regulating vesicle trafficking. Lgl homologs in yeast (Sro7p and Sro77p) and mammals (Lgl1 and Lgl2) bind membrane t-SNAREs (target soluble N-ethylmaleimide attachment protein receptors) that mediate fusion of post-Golgi transport vesicles to target membranes (Lehman et al., 1999; Müsch et al., 2002), suggesting a link between Lgl and polarized exocytosis. Sro7p also interacts with the exocyst complex (Zhang et al., 2005), which tethers vesicles to the plasma membrane, and Sec4p (Grosshans et al., 2006), a member of the Rab family of GTPases that regulate vesicle trafficking and exocyst function. Recently, mammalian Lgl1 was shown to activate Rab10 to control vesicle trafficking during neuronal axon growth (Wang et al., 2011b).

Despite the involvement of Lgl proteins in crucial cellular processes, functions for Lgl during early vertebrate embryonic development remain largely unknown. Although Lgl1 and Lgl2 are widely expressed in the mouse embryo (Klezovitch et al., 2004), knockout of *Lgl1* (*Llgl1* – Mouse Genome Informatics) appears to specifically disrupt brain development and knockout of *Lgl2* (*Llgl2* – Mouse Genome Informatics) only affects placental morphogenesis. *Lgl1*$^{-/-}$ mice show defects in cell polarity and apical-junctional complex formation in neuronal cells and die neonatally from severe hydrocephalus (Klezovitch et al., 2004),

[1]Department of Cell and Developmental Biology, State University of New York, Upstate Medical University, Syracuse, NY 13210, USA. [2]Max Delbrück Center for Molecular Medicine, Robert-Rössle Str. 10, 13125 Berlin, Germany. [3]Institute of Science and Technology Austria, Am Campus 1, A-3400, Klosterneuburg, Austria. [4]Department of Neurobiology and Anatomy, University of Utah School of Medicine, Salt Lake City, UT 84112, USA.

*Author for correspondence (amackj@upstate.edu)

Accepted 30 January 2013

whereas *Lgl2*$^{-/-}$ mice are born small, but develop into normal adults (Sripathy et al., 2011). In zebrafish, a loss-of-function *lgl2* mutant (*penner*) develops epidermal defects at 4 days post-fertilization due to an absence of hemidesmosomes and hyperproliferation in the basal epidermis (Sonawane et al., 2005), and co-knockdown studies have shown that Lgl1 and Lgl2 redundantly control the epithelial organization of the lateral line organ (Hava et al., 2009). These tissue-specific and/or late-appearing phenotypes suggest that some Lgl functions during embryogenesis are masked by redundancy or maternal expression.

In this study, depletion of both maternal and zygotic Lgl2 expression in the early zebrafish embryo has uncovered roles for Lgl2 in the development of ciliated epithelia in Kupffer's vesicle (KV), as well as in otic vesicles and pronephric ducts. Analyses of KV morphogenesis revealed that loss of Lgl2 function disrupted formation of both the cilia and the lumen. Consistent with these defects, left-right patterning was disrupted in Lgl2-depleted embryos, identifying a role for Lgl2 in left-right axis specification. Focusing on the role of Lgl2 in lumen formation, we found that Lgl2 genetically interacted with the GTPase Rab11a to regulate E-cadherin (also known as Cadherin 1, epithelial) at cell-cell contacts. These results identify new functions for Lgl proteins in the vertebrate embryo and implicate Lgl2 in polarized vesicle trafficking, which is essential for development of organs with motile cilia.

MATERIALS AND METHODS

Zebrafish

Wild-type TAB zebrafish (*Danio rerio*) and transgenic *Tg(sox17:GFP)* (Sakaguchi et al., 2006) and *Tg(cmlc2:GFP)* (Huang et al., 2003) zebrafish were obtained from the Zebrafish International Resource Center (ZIRC). *Tg(shh:GFP)* zebrafish (Haga et al., 2009) were a kind gift from Shao Jun Du. Additional transgenic lines were *Tg(dusp6:memGFP)*^{pt19} (Wang et al., 2011a) and *Tg(β-actin:Lyn-TdTomato)* (J.C., unpublished). Embryos were staged as described (Kimmel et al., 1995).

Whole-mount *in situ* RNA hybridization

PCR-amplified *lgl2* cDNA was inserted into the pCRII TOPO vector. *lgl2* and previously described *sox17*, *spaw*, *lft1* and *shha* cDNA constructs (Alexander and Stainier, 1999; Long et al., 2003; Bisgrove et al., 1999; Krauss et al., 1993) were used to generate *in vitro*-synthesized RNA probes labeled with digoxygenin (Roche DIG RNA Labeling Kit). *In situ* RNA hybridizations were performed as described (Gao et al., 2010).

Embryo injections

Morpholino oligonucleotides (MOs) were obtained from Gene Tools, LLC. Two previously described MOs were used to block Lgl2 translation: Lgl2 MO-1 (5′-GCCCATGACGCCTGAACCTCTTCAT-3′) (Sonawane et al., 2009) and Lgl2 MO-2 (5′-AGCCGGGACTCAAACTGCCCTCTCT-3′) (Hava et al., 2009). Rab11a MO (5′- GTATTCGTCGTCTCG-TGTCCCCAT-3′) has also been previously characterized (Westlake et al., 2011). MOs were injected between the 1- and 2-cell stages to allow the MO to be distributed to all embryonic cells. Optimal MO doses used (unless otherwise stated) were: 4.4 ng of Lgl2 MO-1, 2.5 ng of Lgl2 MO-2 and 2 ng of Rab11a MO. All MOs were co-injected with 4 ng p53 MO (5′-GCGCCATTGCTTTGCAAGAATTG-3′) to mitigate off-target effects (Robu et al., 2007). Sub-optimal MO doses used were: Lgl2 MO-1^{low}=1.7 ng and Rab11a MO^{low}=0.8 ng. Co-injection of these two MOs at their sub-optimal levels was performed at 1- to 2-cell stages. To conduct rescue experiments, full-length zebrafish *lgl2* was PCR amplified from a zebrafish cDNA library and cloned into pCS2+ vector. Seven bases were changed in the MO binding site to make the mRNA MO resistant. This cDNA was used to synthesize capped mRNA using mMessage mMachine (Ambion) that was purified using Bio-Gel P-6 Micro Bio Spin columns (BioRad). Titration of synthetic capped *lgl2* mRNA was performed to determine the concentration that resulted in minimal embryo defects. For Lgl2 rescue experiments, Lgl2 MO-1 was co-injected with 150 pg *lgl2* mRNA or 150 pg mRNA encoding an Lgl2:EYFP fusion protein (see below), and Lgl2 MO-2 was co-injected with 100 pg *lgl2* mRNA. For Rab11a rescue experiments, zebrafish *rab11a* with five base changes in the MO binding site was amplified from cDNA and cloned into pCS2+ vector. *In vitro* synthesized mRNA (mMessage mMachine; 100 pg) was co-injected with Rab11a MO at the 1-cell stage for rescue experiments. All MO and rescue data are pooled from at least three independent experiments. To generate an Lgl2:EYFP fusion construct, the protein coding sequence of *lgl2* was inserted upstream of EYFP in the PCS2+ vector using *Cla*I and *Xho*I restriction sites. The *lgl2* stop codon was mutated to cysteine using the QuikChange Site-directed Mutagenesis Kit (Stratagene) to create the fusion protein. To visualize fusion protein localization, 200 pg of *in vitro* synthesized mRNA (mMessage mMachine) was injected into embryos.

Immunohistochemistry and microscopy

Primary antibodies used were: mouse anti-acetylated tubulin (1:200, Sigma), rabbit anti-aPKC (1:100, Santa Cruz), mouse anti-E-cadherin (1:200, BD Transduction Laboratories), rabbit anti-Lgl2 (1:500, a kind gift from Dr Mahendra Sonawane) (Sonawane et al., 2009), mouse anti-ZO-1 (1:200, Invitrogen) and rabbit anti-GFP (1:200, Molecular Probes). Embryos were fixed in 4% paraformaldehyde in PBS with 0.25% Triton X-100 at 4°C overnight and then de-chorionated in 1× PBS. Embryos were permeabilized in blocking solution containing 1× PBS, 0.5% Triton X-100 and 5% goat serum for 4 hours. Primary antibodies were diluted in fresh blocking solution and incubated with embryos at 4°C overnight and then washed in PBS with 0.5% Triton X-100 (three 30-minute washes) at room temperature. AlexaFluor 488-, 568- and 647-conjugated anti-rabbit and anti-mouse secondary antibodies (Molecular Probes) were used at 1:200 in 5% goat serum. AlexaFluor 488 and Rhodamine Phalloidin (Molecular Probes) were each diluted at 1:200 from stock and incubated together with the secondary antibody at 4°C overnight. The stained embryos were then washed in PBS with 0.5% Triton X-100 (three 30-minute washes) at room temperature. Image acquisition was performed using a Perkin-Elmer UltraVIEW Vox spinning disk confocal microscope or an SP5 Leica laser scanning confocal microscope. Image analyses, including quantification of KV cell number (GFP), KV cilia number and length (acetylated tubulin) and KV lumen area at the middle focal plane of KV (largest KV area based on aPKC staining), were performed using ImageJ software. ImageJ was also used to quantify E-cadherin staining at cell junctions. The mean gray level (per pixel) was determined along continuous lateral membranes (adherens junctions) >5 μm starting from the apical region of KV cells. This mean gray level (fluorescence intensity) was normalized to 1 with reference to the MO control embryos.

Analysis of KV morphogenesis and KV volume

Double-transgenic *Tg(sox17:GFP; β-actin:Lyn-TdTomato)* embryos were generated by crossing *Tg(sox17:GFP)* and *Tg(β-actin:Lyn-TdTomato)* parents. Uninjected control embryos or embryos injected with 4 ng Lgl2 MO-2 were mounted in 0.7% low melting temperature agarose at the 1-somite stage and then imaged on a Lavision Biotec TrimScope II 2-photon with optical parametric oscillator (OPO) using a Zeiss 20× 1.0 water dipping lens (Olympus BX51 WI stand). Live embryos were maintained at 28.5°C and images were captured every 450 seconds. Four-dimensional datasets were processed using Imaris software (Bitplane) to correct for KV drift. The coronal plane was exported and assembled into a movie after contrast adjustment. KV lumen volume was quantified at the 8-somite stage using Imaris software. Taking a parallel approach, KV was imaged at the 8-somite stage in live *Tg(dusp6:memGFP)* embryos using spinning disk confocal (Perkin Elmer) microscopy. ImageJ software was used to create a contrasting region of interest (ROI) corresponding to the KV lumen. This ROI was imported into Volocity software (Perkin Elmer) to measure its volume.

Statistics

All statistical analyses were carried out using one-factor ANOVA and Fisher's least significant difference post-hoc test. *P*-values <0.05 were considered to be statistically significant.

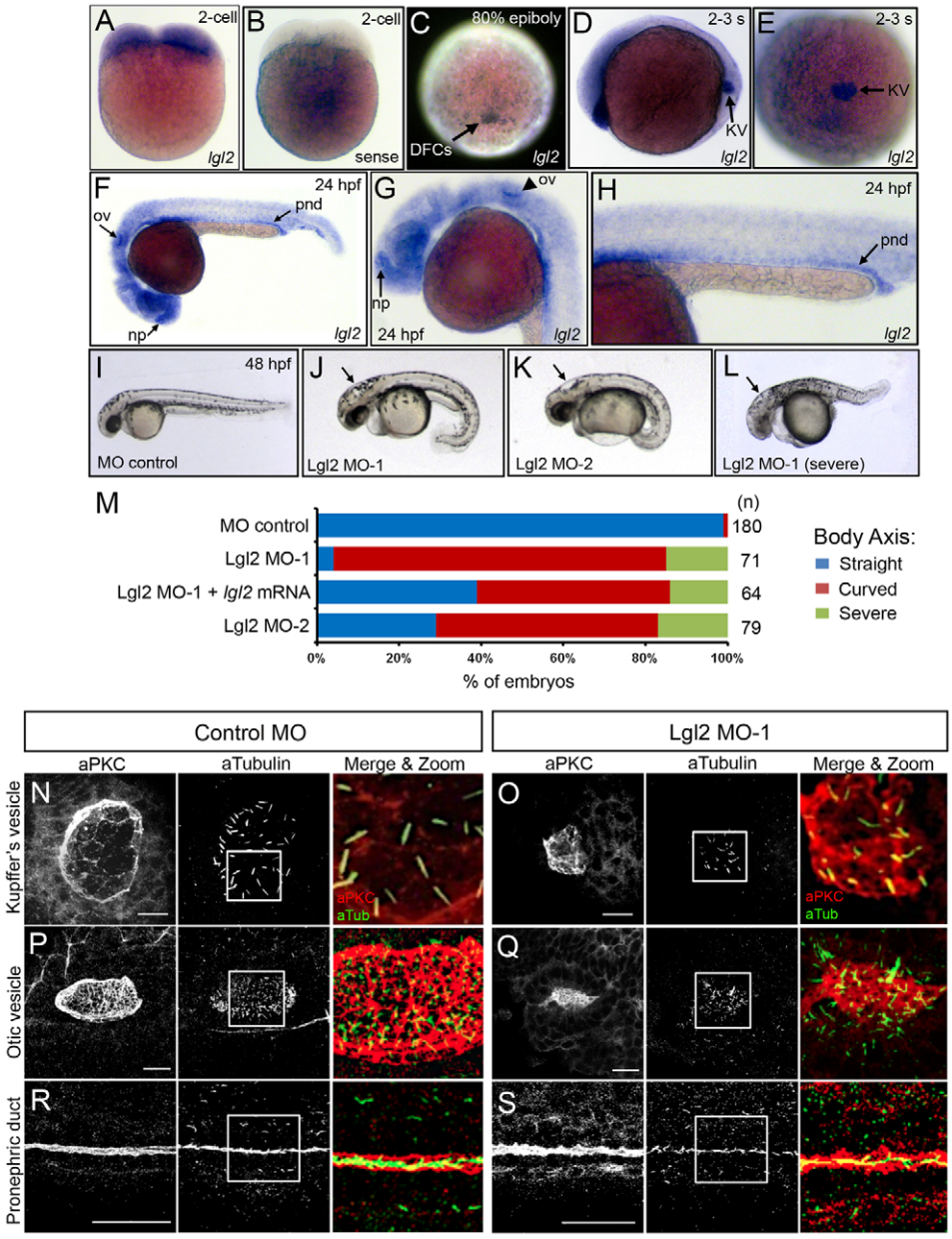

Fig. 1. Lgl2 controls development of ciliated organs. (**A-H**) Whole-mount RNA *in situ* hybridizations. At the 2-cell stage, antisense *lgl2* probes show that *lgl2* mRNA is maternally supplied (A). Control *lgl2* sense probes showed little background staining (B). *lgl2* expression localized in the enveloping layer and dorsal forerunner cells (DFCs) at the 80% epiboly stage (C) and was prominently expressed in Kupffer's vesicle (KV) at the 2-3 somite(s) stages (D,E). At 24 hpf, *lgl2* is highly expressed in the ciliated nasal placodes (np), otic vesicles (ov) and pronephric ducts (pnd) (arrows in F). G and H show higher magnification images of *lgl2* expression in the nasal placode and otic vesicle (G) and pronephric duct (H). (**I-L**) Embryo morphology at 2 dpf. Control embryos (I) had a straight body, whereas Lgl2 MO-1 (J) and Lgl2 MO-2 (K) embryos often showed a curved body. Lgl2 MO embryos also developed hydrocephalus (arrows in J-L) and in some cases had additional severe axial defects (L). (**M**) Percentage of embryos with body axis defects. *n*, number of embryos analyzed. (**N-S**) Fluorescence immunostaining using aPKC antibodies (red) to mark apical membranes of epithelial cells and acetylated tubulin antibodies (green) to label cilia revealed defects in the development of ciliated epithelia in KV (N,O), otic vesicles (P,Q) and pronephric ducts (R,S) in Lgl2 MO embryos (O,Q,S) relative to controls (N,P,R). White boxes indicate areas enlarged in 'Merge & Zoom' panels. Scale bars: 20 μm.

RESULTS

Lgl2 regulates development of ciliated organs

The zebrafish *penner* mutant has revealed roles for Lgl2 in the epidermis at 4-5 days post-fertilization (dpf) (Reischauer et al., 2009; Sonawane et al., 2005; Sonawane et al., 2009), but the pronounced expression of Lgl2 during earlier zebrafish development suggested additional roles for this protein. RNA *in situ* hybridization analysis showed that *lgl2* is maternally supplied (Fig. 1A,B) as previously reported (Sonawane et al., 2005). At the 80% epiboly stage [~8 hours post-fertilization (hpf)], *lgl2* expression was detected in cells of the enveloping layer and was strongly expressed in dorsal forerunner cells (DFCs) that give rise to KV (Cooper and D'Amico, 1996; Melby et al., 1996) (Fig. 1C). At the 2- to 3-somite stages (~11 hpf), *lgl2* was prominently expressed in ciliated KV cells (Fig. 1D,E). At 24 hpf, *lgl2* showed a basal level of expression, with higher expression in organs that contain motile cilia, including nasal placodes, otic vesicles and pronephric ducts (Fig. 1F-H). These analyses suggest that Lgl2 functions in the development of ciliated organs.

To determine the role of Lgl2 during early zebrafish development, we used two previously described antisense morpholino oligonucleotides (MOs) designed to block translation of *lgl2* mRNA and to knock down both maternal and zygotic Lgl2 protein expression. Embryos injected with Lgl2 MO-1 (Sonawane et al., 2005) showed dose-dependent defects, including a curved body axis phenotype at 48 hpf (Fig. 1J,M), similar to some zebrafish cilia mutants (Ferrante et al., 2009; Fogelgren et al., 2011; Kramer-Zucker et al., 2005), and hydrocephalus (Fig. 1J, arrow) that is associated with defects in ependymal cilia (Kramer-Zucker et al., 2005). In some cases, embryos showed more severe phenotypes, including a dramatically shortened body axis (Fig. 1L,M). Lgl2 MOs were co-injected with p53 MO to avoid off-target effects and embryos injected with p53 MO alone (MO control injection) appeared normal at 48 hpf (Fig. 1I,M). Injecting Lgl2 MO-2 (Hava et al., 2009) also resulted in dose-dependent curved body defects and hydrocephalus (Fig. 1K,M). Co-injecting sub-optimal levels of these two different MOs recapitulated these effects (supplementary

material Fig. S1A) and injecting 150 pg of MO-resistant *lgl2* mRNA partially rescued Lgl2 MO body axis defects, indicating the specificity of this phenotype (Fig. 1M). Early embryonic phenotypes observed in Lgl2 MO-injected embryos, but not seen in *penner* zygotic mutants, are consistent with MO interference with both maternal and zygotic *lgl2* expression (Sonawane et al., 2005).

Next, development of ciliated organs was assessed in Lgl2 MO embryos by conducting immunofluorescence staining using aPKC antibodies to detect apical epithelial cell membranes and acetylated tubulin (aTubulin) antibodies to label cilia (Amack et al., 2007). In KV at the 8-somite stage, aPKC localized at apical membranes in Lgl2 MO embryos, indicating that apical-basal polarity was intact. However, the lumen of KV was smaller, and the number and length of KV cilia appeared to be reduced relative to controls (Fig. 1N,O). Similarly, at 24 hpf, otic vesicle lumen size was reduced in Lgl2 MO embryos compared with control embryos, and the number and length of motile cilia appeared to be reduced (Fig. 1P,Q). Also at 24 hpf, pronephric duct cilia appeared to be shorter and more disorganized in Lgl2 MO embryos, compared with the densely packed network of cilia in the lumen of controls (Fig. 1R,S). Together, these results indicate that Lgl2 is involved in the development of organs containing motile cilia.

Lgl2 is required for normal ciliogenesis and lumenogenesis in Kupffer's vesicle

To study the function of Lgl2 in more detail, we analyzed the development of KV, the first ciliated organ to appear in the zebrafish embryo. KV is analogous to ciliated structures in other vertebrates, including the ventral node in mouse (Nonaka et al., 1998), gastrocoel roof plate in frog (Schweickert et al., 2007) and notochordal plate in rabbit (Okada et al., 2005), that generate an asymmetric fluid flow involved in establishing left-right asymmetry in the embryo. KV is derived from dorsal forerunner cells that cluster near the end of gastrulation, become polarized epithelial KV cells and assemble one motile cilium per cell, which protrudes from the apical surface into a nascent lumen (Cooper and D'Amico, 1996; Essner et al., 2005; Kramer-Zucker et al., 2005). The lumen then expands during somitogenesis stages and the cilia beat to generate coordinated flow (Essner et al., 2005; Kramer-Zucker et al., 2005). To visualize KV, we used transgenic *Tg(sox17:GFP)* embryos, which express GFP in KV cells (Sakaguchi et al., 2006), and labeled cilia with acetylated tubulin antibodies (Fig. 2A,B). We found that the number (Fig. 2C) and length (Fig. 2D) of KV cilia were significantly reduced in Lgl2 MO embryos. In addition, the size of the KV lumen area measured at the middle focal plane of KV (the largest KV area) was smaller in Lgl2 MO embryos (Fig. 2E). Consistent with reduced KV lumen area in fixed Lgl2 MO embryos, measurements of the 3D volume of KV lumen in live embryos with GFP-labeled KV cells indicated that KV volume was significantly reduced in Lgl2 MO embryos relative to controls (supplementary material Fig. S2A). Despite the small lumen size, ZO-1 and F-actin, markers of apical membrane domains, were enriched at apical surfaces lining the lumen in Lgl2 MO embryos, similar to controls (supplementary material Fig. S2B,C), indicating that KV cells in Lgl2-depleted embryos establish apical-basal polarity. KV lumen and cilia defects in Lgl2 MO embryos were partially rescued by *lgl2* mRNA (Fig. 2C-E), indicating that these effects were specific to loss of Lgl2 function.

The reduction in KV lumen size and number of KV cilia in Lgl2 MO embryos (Fig. 2B) suggested that there might be fewer cells in KV. Analysis of *sox17* expression in precursor DFCs during epiboly showed that the size of the DFC domain was similar in Lgl2 MO

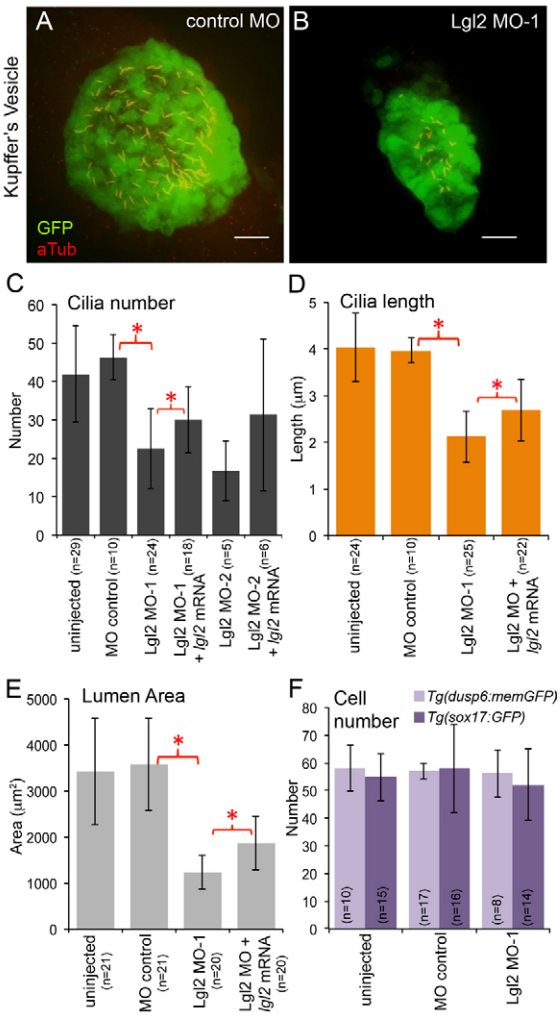

Fig. 2. Lgl2 depletion disrupts KV lumen and cilia formation. (**A**,**B**) Ciliated KV cells were labeled by acetylated tubulin immunostaining (red) and GFP expression (green) in *Tg(sox17:GFP)* embryos injected with control (A) or Lgl2 (B) MO. Scale bars: 20 μm. (**C-E**) KV cilia number (C), KV cilia length (D) and KV lumen size (E) were significantly reduced in Lgl2 MO embryos compared with MO control and uninjected controls. *lgl2* mRNA partially rescued each of these defects. (**F**) The number of KV cells was similar among control and Lgl2 MO embryos in *Tg(dusp6:memGFP)* and *Tg(sox17:GFP)* transgenic lines. Error bars indicate s.d. *n*, number of embryos analyzed. *P<0.05.

embryos and controls. In a subset of Lgl2 MO embryos (23%, n=56), DFCs were not tightly clustered at 90% epiboly (supplementary material Fig. S3B-C), suggesting adhesion or migration defects that might affect the number of cells that incorporate into KV. However, counting GFP$^+$ KV cells at the 8-somite stage in either *Tg(sox17:GFP)* embryos or a second transgenic line, *Tg(dusp6:memGFP)*, that expresses plasma membrane localized GFP in KV cells (Wang et al., 2011a), revealed that the number of cells was similar in both control and Lgl2 MO embryos (Fig. 2F). Thus, Lgl2 knockdown disrupted lumen and cilia formation without affecting KV cell number.

Defective lumen formation in Lgl2 MO embryos suggested that the dynamics of KV morphogenesis might be disturbed. Therefore, time-lapse experiments were performed using *Tg(dusp6:memGFP)* embryos (data not shown) or double transgenic *Tg(sox17:GFP; β-*

actin:Lyn-TdTomato) embryos, in which cell membranes are labeled by Lyn-TdTomato (supplementary material Movie 1). An optical cross-section through the middle plane of KV was analyzed to visualize lumen formation between the 1- and 5-somite stages. In controls, GFP^+ KV cells were dynamic and the lumen expanded during development (supplementary material Movie 1). Consistent with results in fixed embryos (Fig. 2B,E), Lgl2 knockdown disrupted lumenogenesis in live embryos (n=4/4 movies). KV cells formed a rosette-like structure in Lgl2 MO embryos, but the lumen failed to expand as it does in controls (supplementary material Movie 1). In addition, some KV cells in Lgl2 MO embryos appeared to detach from neighboring cells, suggesting defects in KV cell adhesion. Taken together, our analyses show Lgl2 regulates lumen formation and cilia formation in KV.

Consistent with disruption of KV development, Lgl2 MO embryos showed left-right patterning defects. Asymmetric looping of the heart, which normally looped to the right in controls, was often reversed or failed to loop in Lgl2 MO-1 and Lgl2 MO-2 embryos (Fig. 3A,B). These heart-looping defects were also observed in embryos co-injected with sub-optimal doses of the two different Lgl2 MOs (supplementary material Fig. S1B) and were partially rescued by *lgl2* mRNA (Fig. 3B). Injecting *lgl2* mRNA alone also disrupted heart looping (Fig. 3B), suggesting that normal left-right asymmetry requires tight regulation of Lgl2 activity. Examination of asymmetric expression of the *Nodal*-related gene *southpaw* (*spaw*), which is normally expressed in the left lateral plate mesoderm (Long et al., 2003), revealed dose-dependent abnormalities in Lgl2 MO embryos, including right-sided, bilateral and absent *spaw* expression (Fig. 3C,D). Analysis of additional asymmetrically expressed genes, *pitx2c* (Essner et al., 2000) and *cyclops* (Rebagliati et al., 1998) (also known as *ndr2*), and markers of the embryonic midline, *sonic hedgehog* (Krauss et al., 1993) and *lefty1* (Bisgrove et al., 1999), indicated that Lgl2 depletion altered left-right patterning (supplementary material Table S1) without disrupting the midline that provides a barrier between left and right sides (supplementary material Fig. S4). These results uncover a crucial role for Lgl2 in left-right patterning of the embryo.

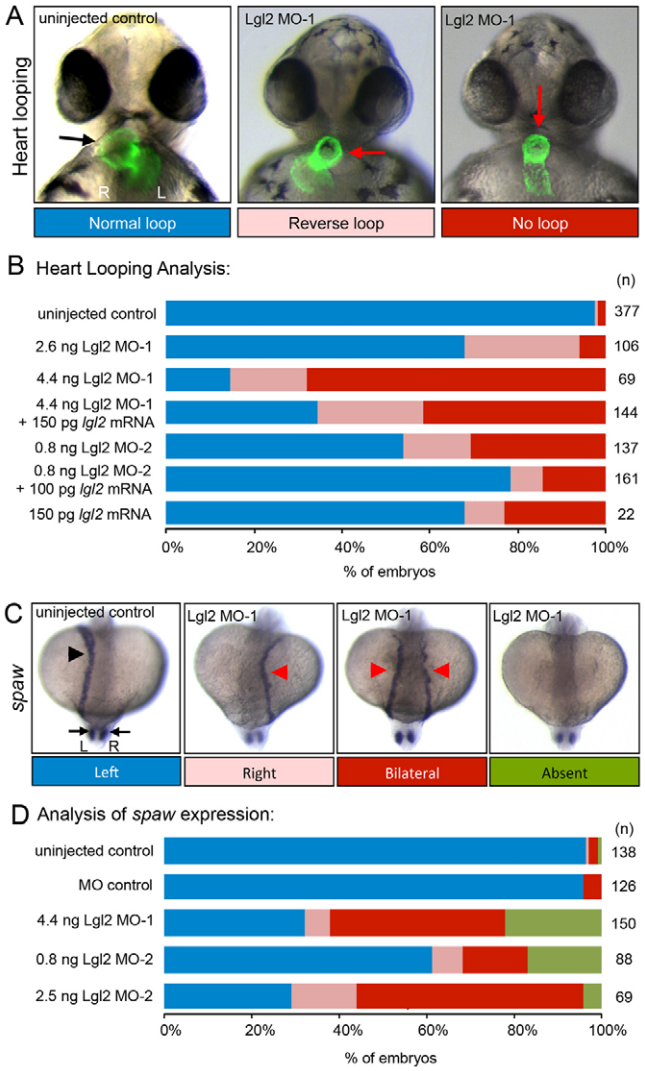

Fig. 3. Lgl2 is required for normal left-right asymmetry. (**A**) Asymmetric heart looping at 2 dpf visualized in *Tg(cmlc2:GFP)* transgenic embryos that express GFP in the heart. In control embryos, the heart (black arrow) looped to the right, whereas Lgl2 MO knockdown often resulted in reversed or no heart looping (red arrows). (**B**) Percentage of embryos with heart-looping defects. Injecting a lower dose of Lgl2 MO-1 revealed that looping defects are dose dependent, and co-injecting *lgl2* mRNA partially rescued Lgl2 MO-1 and Lgl2 MO-2 heart defects. Injecting *lgl2* mRNA alone also disrupted heart looping. (**C**) RNA *in situ* hybridization analysis of *spaw* expression, which was detected in left lateral plate mesoderm (LPM) (arrowhead) and bilaterally in the tail (arrows) at 14 hpf in controls. Lgl2 MO embryos showed disrupted LPM *spaw* expression, including right-sided, bilateral and absent expression (red arrowheads). (**D**) Analysis of LPM *spaw* expression in control and Lgl2 MO embryos. *n*, number of embryos analyzed. L, left; R, right.

Lgl2 is necessary for E-cadherin accumulation at basolateral membranes during Kupffer's vesicle morphogenesis

To assess where Lgl2 localizes in ciliated KV cells, antibodies specific for Lgl2 (Sonawane et al., 2009) were used in immunofluorescence staining experiments. In wild-type embryos, Lgl2 localized at the basolateral membrane of KV cells and was excluded from the apical domain marked by phalloidin staining of cortical F-actin (Fig. 4A). Lgl2 immunostaining was significantly reduced in KV cells of Lgl2 MO depleted embryos relative to controls (supplementary material Fig. S5), providing evidence for antibody specificity and MO efficacy. Interestingly, Lgl2 was also observed in some KV cilia, either throughout the cilium or at the cilium base (supplementary material Fig. S6A). To characterize this ciliary localization further, we analyzed motile ependymal cilia in the spinal cord and found Lgl2 localized to cell membranes and associated with a subset of these cilia (supplementary material Fig. S6B,C). As a second approach to study Lgl2 localization, the coding sequence for full-length Lgl2 was fused to enhanced yellow fluorescent protein (EYFP) cDNA to generate a fluorescent-tagged Lgl2:EYFP fusion protein. Similar to endogenous Lgl2, Lgl2:EYFP showed basolateral membrane localization in wild-type embryos (Fig. 4B). Expression of Lgl2:EYFP rescued axial phenotypes and heart-looping defects in Lgl2 MO embryos with similar efficiency as the wild-type Lgl2 (supplementary material Fig. S7), suggesting that the fusion protein is functional. Lgl2:EYFP was not detected in KV cilia, potentially owing to low abundance or access restrictions. However, Lgl2:EYFP was found to localize near the adherens junction protein E-cadherin (Fig. 4B), which is known to play important roles in KV development (Matsui et al., 2011; Oteíza et al., 2008; Oteiza et al., 2010).

Because the relationship between lumenogenesis and ciliogenic programs remain poorly understood, such that reduced ciliogenesis

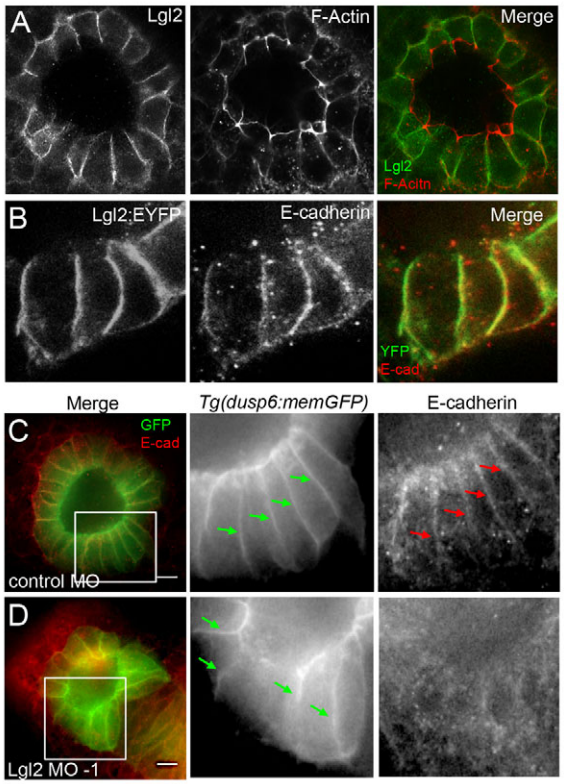

Fig. 4. Lgl2 localizes to basolateral membranes in KV cells and E-cadherin is disrupted in Lgl2 knockdown embryos. (**A**) Fluorescence immunostaining using Lgl2 antibodies showed Lgl2 localized at basolateral membranes of KV cells and was excluded from the apical domain enriched with phalloidin staining of filamentous actin (F-Actin). (**B**) Lgl2:EYFP fusion protein also localized at basolateral membranes of KV cells and near E-cadherin staining. (**C**,**D**) In MO control *Tg(dusp6:memGFP)* embryos, E-cadherin localized at lateral membranes (C), whereas Lgl2 MO knockdown reduced membrane accumulation of E-cadherin (D). Boxes indicate enlarged regions shown in the individual channels. Arrows point out representative lateral membranes. Scale bars: 20 μm.

may be secondary to disrupted lumen formation, we focused on the role of Lgl2 in lumenogenesis. To begin to understand how Lgl2 regulates KV lumen formation, we analyzed E-cadherin. Lgl2 and E-cadherin have been previously shown to function antagonistically to control hemidesmosome formation in basal epidermal cells (Sonawane et al., 2009), and membrane localization of E-cadherin in the epidermis was disrupted in *lgl2* mutant embryos (Reischauer et al., 2009). In addition, knockdown of E-cadherin in the DFC/KV cell lineage resulted in KV morphogenesis defects similar to those observed in Lgl2 MO embryos, including altered DFC clustering and small KV lumen size (Matsui et al., 2011; Oteíza et al., 2008; Oteiza et al., 2010). To study the relationship of Lgl2 with E-cadherin in KV, we performed immunostaining using E-cadherin antibodies and compared control and Lgl2 MO embryos. In control *Tg(dusp6:memGFP)* embryos, GFP labeled well-defined KV cell membranes and E-cadherin localized at lateral membrane domains (Fig. 4C). By contrast, KV cell membranes appeared disorganized in Lgl2 MO embryos and E-cadherin was reduced along the lateral domain (Fig. 4D). This indicates that Lgl2 is necessary for E-cadherin accumulation in KV membranes and that disruption of E-cadherin contributes to KV lumen defects in Lgl2 MO embryos.

Lgl2 genetically interacts with Rab11a to regulate E-cadherin and Kupffer's vesicle morphogenesis

To gain further mechanistic insight into how Lgl2 controls KV morphogenesis, we next tested whether Lgl2 is involved with vesicle trafficking machinery. Interestingly, the Rab family GTPase Rab11, which regulates recycling endosomes and vesicle trafficking from the trans-Golgi (Das and Guo, 2011), controls cilia length (Knödler et al., 2010) and the sorting and basolateral transport of E-cadherin in mammalian cell cultures (Lock and Stow, 2005). In zebrafish, MO knockdown of Rab11a has been recently shown to reduce KV lumen size (Westlake et al., 2011), similar to the KV phenotype observed in Lgl2 MO embryos. Thus, we hypothesized that Lgl2 genetically interacts with Rab11a to regulate KV development. To study Rab11a, we obtained the Rab11a MO and used an optimal dose to reduce KV size (supplementary material Fig. S8A-C) as previously reported (Westlake et al., 2011). Importantly, rescue experiments previously demonstrated this effect is specific to Rab11a depletion (Westlake et al., 2011). Quantification of KV lumen size revealed a significant difference between Rab11a MO embryos and controls (supplementary material Fig. S8D). In Rab11a MO embryos with small KVs, the cilia number and length were reduced (supplementary material Fig. S8E,F), suggesting that, similar to Lgl2, Rab11a is necessary for KV ciliogenesis. Consistent with these KV defects, cardiac left-right asymmetry was altered in Rab11a MO embryos (supplementary material Fig. S8G). Co-injecting MO-resistant mRNA encoding zebrafish Rab11a partially rescued left-right asymmetry defects in Rab11a morphants (supplementary material Fig. S8G), indicating that these phenotypes are specific to Rab11a knockdown.

The phenotypic similarities between Lgl2- and Rab11a-depleted embryos supported our hypothesis that Lg2 and Rab11a cooperate during KV morphogenesis, potentially to regulate vesicle trafficking of proteins essential for cilia formation and/or targeting E-cadherin to cell membranes. To test this hypothesis, genetic interaction experiments were conducted by co-injecting lower MO doses (Lgl2 MO-1^{low} + Rab11a MO^{low}) to determine whether partial knockdown of both Lgl2 and Rab11a resulted in synergistic effects on KV development. Although Lgl2 MO-1^{low} or Rab11a MO^{low} alone had modest effects on KV development, co-injection significantly reduced KV lumen volume (Fig. 5A,C). In contrast to lumen defects, the number and length of KV cilia were not affected in Lgl2 MO-1^{low} + Rab11a MO^{low} embryos (Fig. 5B,D,E). This indicates that KV lumenogenesis defects can be genetically uncoupled from cilia phenotypes.

We also investigated whether Rab11a genetically interacts with Lgl2 to regulate E-cadherin at lateral membranes of KV cells. *Tg(dusp6:memGFP)* embryos injected with Lgl2 MO-1^{low} or Rab11a MO^{low} showed accumulation of E-cadherin at KV cell junctions, as observed in control embryos (Fig. 6A-C). Quantification of E-cadherin staining along KV membranes in several embryos indicated that levels were modestly reduced in embryos injected with Lgl2 MO-1^{low} or Rab11a MO^{low} relative to controls (Fig. 6E). By contrast, co-injection of Lgl2 MO-1^{low} + Rab11a MO^{low}, which disrupted lumen formation, showed a more dramatic reduction of E-cadherin immunostaining at the lateral domain of KV cells (Fig. 6D) that was significantly different from embryos injected with Lgl2 MO-1^{low} or Rab11a MO^{low} alone (Fig. 6E). Taken together, our results show that genetic interactions between Lgl2 and Rab11a regulate E-cadherin and are crucial for normal KV lumenogenesis.

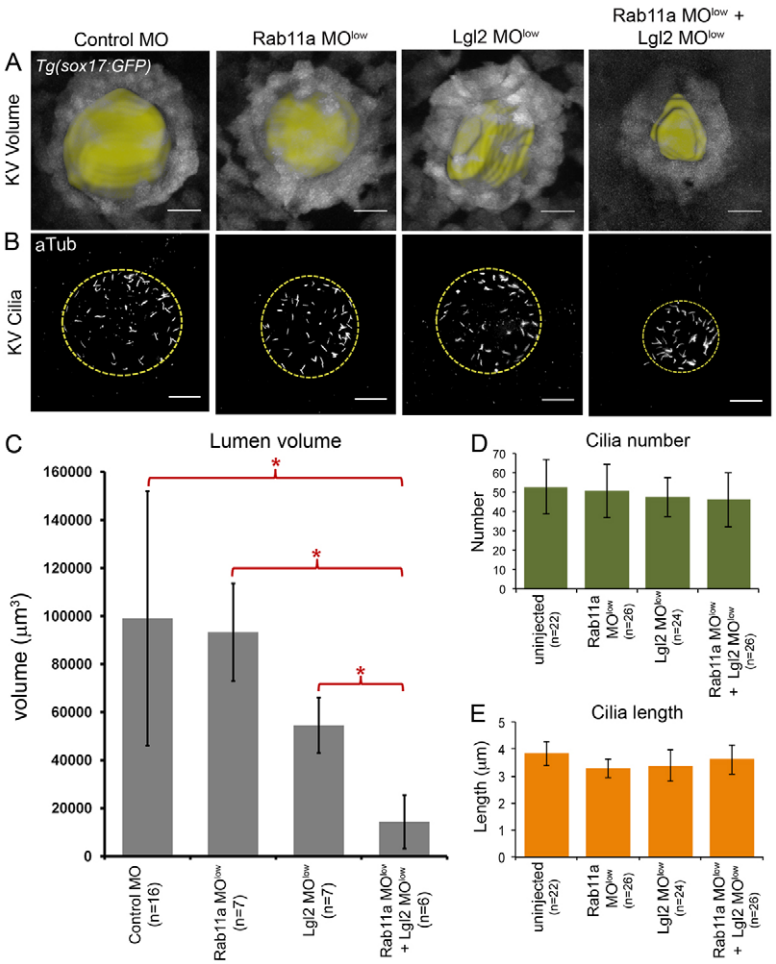

Fig. 5. Genetic interaction between Lgl2 and Rab11a regulates KV lumen formation uncoupled from ciliogenesis. (**A**,**B**) Images of GFP-labeled KV cells were used to determine KV lumen volumes (pseudocolored yellow) in live *Tg(sox17:GFP)* embryos (A) and acetylated tubulin antibodies were used to stain KV cilia (B) in MO control embryos and embryos injected with sub-optimal Rab11a MO^{low}, Lgl2 MO^{low} or co-injected with Rab11a MO^{low} + Lgl2 MO^{low}. The dashed circle outlines the approximate boundary of KV lumen. Scale bars: 20 μm. (**C**) Average volume of KV lumen at the 8-somite stage. (**D**,**E**) Analysis of KV cilia number (D) and length (E) showed that KV cilia were not significantly affected in Rab11a MO^{low} + Lgl2 MO^{low} embryos. Error bars indicate s.d. *n*, number of embryos analyzed. **P*<0.05.

DISCUSSION

Motile cilia facilitate a number of crucial functions, including airway clearance, cerebrospinal fluid flow and the placement of organs along the left-right body axis. Here, we used KV in the zebrafish embryo to examine the role of Lgl2 in the development of ciliated organs. Lgl proteins are involved in several important biological processes, yet functions for Lgl during vertebrate development are unclear. We show that Lgl2 is involved in the genesis of motile cilia and cooperates with the Rab11a GTPase to regulate E-cadherin accumulation at cell-cell junctions and lumen formation. Importantly, reduction of both Lgl2 and Rab11a expression disrupted lumenogenesis without affecting ciliogenesis in KV, indicating that these processes can be uncoupled. Our study indicates that Lgl2 interacts with vesicular trafficking machinery to control lumen development in ciliated organs and that disrupting this pathway does not provide feedback that inhibits ciliogenesis.

New roles for Lgl2 during vertebrate development

The mechanism(s) by which Lgl proteins function at the molecular level has remained enigmatic, but several studies have used a loss-of-function approach or identified interactions between Lgl and specific protein complexes to shed light on Lgl functions. In this article, we present two novel roles for Lgl2 in ciliated organs: a Rab11a-associated role in lumenogenesis and a second role in ciliogenesis. In addition to lumen-expansion defects in Lgl2-depleted embryos, some KV cells in these embryos had short cilia whereas others were devoid of cilia. This observation indicates Lgl2 is in involved in formation of cilia (ciliogenesis) rather than (or in addition to) regulating cilia length. Cilia-associated phenotypes were not observed in $Lgl1^{-/-}$ or $Lgl2^{-/-}$ knockout mice, but Lgl1 and Lgl2 appear to be co-expressed throughout the early mouse embryo raising the possibility that Lgl1 and Lgl2 function redundantly to control cilia development in mammals. Ciliary defects are also apparently absent in zebrafish *penner* mutants, indicating that maternal Lgl2 compensates for loss of zygotic expression during early development. Our study provides the first evidence that Lgl2 plays early roles in the vertebrate embryo that are important for ciliated epithelium formation, body axis development and left-right patterning.

In *Drosophila* epithelial cells, Lgl proteins are known to interact with Scribbled and Discs large and antagonize the aPKC-Par3-Par6 complex to regulate apicobasal polarity. Loss of Lgl function in *Drosophila* or $Lgl1^{-/-}$ knockout mice disrupts apicobasal polarity and results in hyperproliferation of specific cell types (Gateff, 1978; Klezovitch et al., 2004). Our analyses of apicobasal polarity in ciliated organs (Fig. 1; supplementary material Fig. S2) did not reveal gross defects in Lgl2-depleted embryos. Although malformations of the epithelia made it difficult to detect subtle changes in apical or basolateral membrane domains, the overall polarity appeared similar in Lgl2 MO and control embryos. In zebrafish *penner* mutants, loss of Lgl2 did not alter apicobasal polarity, but disrupted the formation of basally localized hemidesmosomes (Sonawane et al., 2005) and promoted

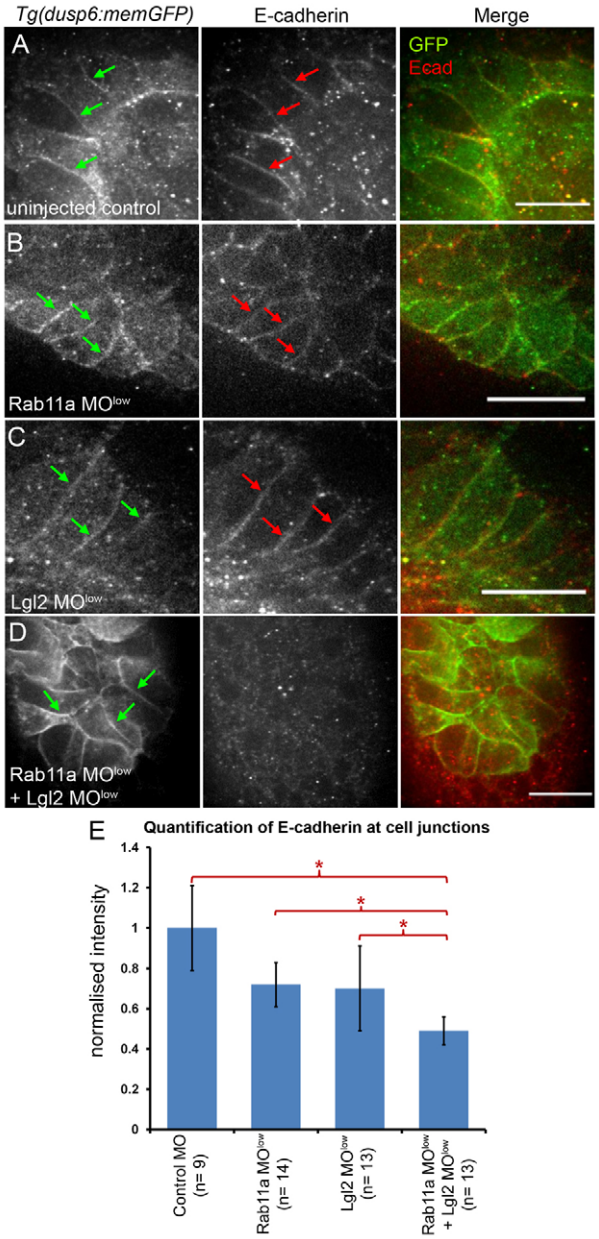

Fig. 6. Lgl2 and Rab11a control E-cadherin accumulation at KV cell junctions. (**A-D**) Optical sections showing E-cadherin immunostaining in KV cells of *Tg(dusp6:memGFP)* embryos. GFP (green arrows) and E-cadherin (red arrows) accumulate at lateral membranes in control (A), Rab11a MO^{low} (B) and Lgl2 MO^{low} (C) embryos. E-cadherin membrane staining was reduced in Rab11a MO^{low} + Lgl2 MO^{low} embryos (D). Scale bars: 20 µm. (**E**) Quantification of E-cadherin staining along lateral KV membranes. Average fluorescence intensities from multiple experiments were normalized to controls. Error bars indicate s.d. *n*, number of embryos analyzed. **P*<0.05.

epithlelial-to-mesenchymal transition (EMT) and over-proliferation of epidermal cells (Reischauer et al., 2009). In our studies of Lgl2-depleted embryos, we did not observe evidence of EMT or hyperproliferation of KV cells. Our results suggest that the functions of Lgl2 during ciliogenesis and lumenogenesis in developing epithelia are distinct from its roles in the zebrafish epidermis.

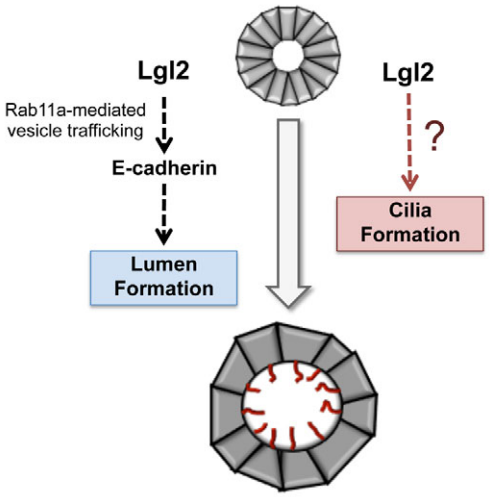

Fig. 7. Working model for how Lgl2 regulates development of ciliated organs. Depletion of Lgl2 disrupted both lumen formation and cilia formation in organs with motile cilia. Our results indicate that Lgl2 interacts with Rab11a-mediated vesicle trafficking to promote E-cadherin accumulation at junctions between ciliated cells in Kupffer's vesicle. Previous studies have shown that E-cadherin is necessary for Kupffer's vesicle formation. Genetic interaction studies between Lgl2 and Rab11a revealed that cilia phenotypes are separable from lumen defects, indicating a second role for Lgl2 regulating cilia formation. Whether Lgl2 interacts with vesicle trafficking during ciliogenesis remains an open question.

How do Lgl2 and Rab11a regulate the development of ciliated organs?

Lgl homologs interact with vesicle-trafficking components and exocytic machinery and are involved in delivering specific proteins to target membranes. Mutations in the yeast Lgl homologs Sro7 or Sro77, which interact with t-SNAREs, disrupt fusion of post-Golgi vesicles with plasma membrane (Gangar et al., 2005; Zhang et al., 2005). In zebrafish, Lgl2 acts synergistically with Clathrin-interactor 1 (Clint1), which binds clathrin-coated components and vesicle-associated SNARE proteins (v-SNAREs) involved in vesicle fusion (Dodd et al., 2009). We propose that Lgl2 mediates polarized vesicle trafficking, which is essential for development of ciliated organs (Fig. 7). This model includes trafficking of E-cadherin to basolateral membranes of KV cells. E-cadherin is highly expressed in the DFC/KV cell lineage (Kane et al., 2005; Oteiza et al., 2010) and is essential for normal KV development (Oteiza et al., 2010). As depletion of E-cadherin in DFC/KV cells disrupts DFC adhesion and KV lumen formation, loss of E-cadherin at basolateral membranes in Lgl2-depleted embryos is likely to be responsible, at least in part, for KV lumen defects. E-cadherin-based adherens junctions might be necessary for epithelial remodeling and/or to maintain epithelial integrity during fluid influx and lumen expansion.

In addition to a role in lumen formation, our functional analyses have uncovered a second role for Lgl2 in cilia formation (Fig. 7). We propose that Lgl2 regulates protein trafficking to cilia, which is necessary for normal ciliogenesis. Our detection of Lgl2 near some (but not all) cilia in fixed tissues (supplementary material Fig. S6) might reflect transient and dynamic localization of Lgl2 with cilia, which would be consistent with a role for Lgl2 in vesicle trafficking to cilia. Although we did not detect Lgl2:EYFP fusion protein associated with cilia in live embryos, generating stable transgenic lines that express Lgl2:EYFP coupled with higher resolution

imaging may be a useful approach to study Lgl2 protein dynamics. In addition, it will be interesting to test our model that cilia formation can be separated from lumen formation by identifying new factors that regulate lumen size and then drawing correlations with ciliogenesis. It will also be interesting to test the role of Lgl2 in ciliogenesis in a cell culture system in the absence of lumenogenesis.

Similar to the roles of Lgl2 we have described in zebrafish, Rab11 mediates ciliogenesis and lumenogenesis in mammalian cells by regulating exocyst function (Bryant et al., 2010; Das and Guo, 2011; Datta et al., 2011; Knödler et al., 2010; Stenmark, 2009). The exocyst protein Sec15 (also known as Exoc6) has been shown to be a downstream effector of Rab11a, and Sec15 knockdown inhibited lumen formation in cultured Madin-Darby canine kidney (MDCK) epithelial cells (Bryant et al., 2010). In polarized MDCK cells, Rab11a is associated with recycling endosomes and is involved in targeting E-cadherin to cell junctions (Desclozeaux et al., 2008; Oztan et al., 2007). Our co-knockdown studies suggest that Lgl2 and Rab11a cooperate in the zebrafish embryo to localize E-cadherin to adherens junctions in KV cells. Thus, it is plausible that Lgl2 regulates the asymmetric distribution of membrane proteins such as E-cadherin via interactions with Rab11a, and potentially the exocyst complex, to regulate polarized KV tissue architecture and remodeling that is coupled with lumenogenesis. It is interesting that this process does not impact cilia formation in KV, indicating that cilia number and length is not influenced by lumen size in this organ. However, we cannot rule out an interaction between Lgl2 and Rab11 that is involved in ciliogenesis, owing to technical reasons (our MO doses may have not been sufficient to uncover such an interaction) or owing to other zebrafish Rab11 proteins, including Rab11al, Rab11ba and Rab11bb (Clark et al., 2011), which may compensate for loss of Rab11a during cilia formation.

In *Drosophila*, Lgl binds to myosin II and negatively regulates myosin activity (Strand et al., 1994), whereas mammalian Lgl2 positively regulates myosin II activity in MDCK cells (Wan et al., 2012). Thus, KV lumen expansion defects in the absence of Lgl2 might be partly due to aberrant actomyosin activity in KV cells. Regulation of actomyosin activity and E-cadherin accumulation may need to be coordinated (Shewan et al., 2005; Smutny et al., 2010) in order to control the KV cell-cell adhesions and contractility necessary for lumen formation. Additional experimental approaches will be needed to try to tease apart the roles of Myosin II in cell adhesion and contractility in ciliated organs and to test whether Lgl2 regulates either of these activities in the embryo.

In summary, this study has revealed new functions for Lgl2 that are important for the formation of ciliated organs and development of the embryo. Lgl2 controls formation and length of motile cilia, cooperates with the vesicle trafficking regulator Rab11a to mediate lumen formation and is necessary for proper left-right patterning and organ laterality. These results provide a framework for future work investigating the role of Lgl2 in vesicle trafficking during embryonic development.

Acknowledgements
We thank members of the Amack lab for helpful discussions and Mahendra Sonawane for donating reagents.

Funding
This work was supported by a National Institutes of Health (NIH) National Research Service Award (NRSA) postdoctoral fellowship; an American Heart Association (AHA) Scientist Development Award; and a National Heart, Lung, and Blood Institute (NHLBI) grant [R01HL095690] to J.D.A. S.A.-S. is supported by a Heisenberg fellowship of the Deutsche Forschungsgemeinschaft (DFG). Deposited in PMC for release after 12 months.

Competing interests statement
The authors declare no competing financial interests.

Supplementary material
Supplementary material available online at
http://dev.biologists.org/lookup/suppl/doi:10.1242/dev.087130/-/DC1

References
Alexander, J. and Stainier, D. Y. (1999). A molecular pathway leading to endoderm formation in zebrafish. *Curr. Biol.* **9**, 1147-1157.
Amack, J. D., Wang, X. and Yost, H. J. (2007). Two T-box genes play independent and cooperative roles to regulate morphogenesis of ciliated Kupffer's vesicle in zebrafish. *Dev. Biol.* **310**, 196-210.
Atwood, S. X. and Prehoda, K. E. (2009). aPKC phosphorylates Miranda to polarize fate determinants during neuroblast asymmetric cell division. *Curr. Biol.* **19**, 723-729.
Betschinger, J., Mechtler, K. and Knoblich, J. A. (2003). The Par complex directs asymmetric cell division by phosphorylating the cytoskeletal protein Lgl. *Nature* **422**, 326-330.
Betschinger, J., Eisenhaber, F. and Knoblich, J. A. (2005). Phosphorylation-induced autoinhibition regulates the cytoskeletal protein Lethal (2) giant larvae. *Curr. Biol.* **15**, 276-282.
Bisgrove, B. W., Essner, J. J. and Yost, H. J. (1999). Regulation of midline development by antagonism of lefty and nodal signaling. *Development* **126**, 3253-3262.
Bryant, D. M., Datta, A., Rodríguez-Fraticelli, A. E., Peränen, J., Martín-Belmonte, F. and Mostov, K. E. (2010). A molecular network for de novo generation of the apical surface and lumen. *Nat. Cell Biol.* **12**, 1035-1045.
Clark, B. S., Winter, M., Cohen, A. R. and Link, B. A. (2011). Generation of Rab-based transgenic lines for in vivo studies of endosome biology in zebrafish. *Dev. Dyn.* **240**, 2452-2465.
Cooper, M. S. and D'Amico, L. A. (1996). A cluster of noninvoluting endocytic cells at the margin of the zebrafish blastoderm marks the site of embryonic shield formation. *Dev. Biol.* **180**, 184-198.
Das, A. and Guo, W. (2011). Rabs and the exocyst in ciliogenesis, tubulogenesis and beyond. *Trends Cell Biol.* **21**, 383-386.
Datta, A., Bryant, D. M. and Mostov, K. E. (2011). Molecular regulation of lumen morphogenesis. *Curr. Biol.* **21**, R126-R136.
Desclozeaux, M., Venturato, J., Wylie, F. G., Kay, J. G., Joseph, S. R., Le, H. T. and Stow, J. L. (2008). Active Rab11 and functional recycling endosome are required for E-cadherin trafficking and lumen formation during epithelial morphogenesis. *Am. J. Physiol. Cell Physiol.* **295**, C545-C556.
Dodd, M. E., Hatzold, J., Mathias, J. R., Walters, K. B., Bennin, D. A., Rhodes, J., Kanki, J. P., Look, A. T., Hammerschmidt, M. and Huttenlocher, A. (2009). The ENTH domain protein Clint1 is required for epidermal homeostasis in zebrafish. *Development* **136**, 2591-2600.
Essner, J. J., Branford, W. W., Zhang, J. and Yost, H. J. (2000). Mesendoderm and left-right brain, heart and gut development are differentially regulated by pitx2 isoforms. *Development* **127**, 1081-1093.
Essner, J. J., Amack, J. D., Nyholm, M. K., Harris, E. B. and Yost, H. J. (2005). Kupffer's vesicle is a ciliated organ of asymmetry in the zebrafish embryo that initiates left-right development of the brain, heart and gut. *Development* **132**, 1247-1260.
Ferrante, M. I., Romio, L., Castro, S., Collins, J. E., Goulding, D. A., Stemple, D. L., Woolf, A. S. and Wilson, S. W. (2009). Convergent extension movements and ciliary function are mediated by ofd1, a zebrafish orthologue of the human oral-facial-digital type 1 syndrome gene. *Hum. Mol. Genet.* **18**, 289-303.
Fogelgren, B., Lin, S. Y., Zuo, X., Jaffe, K. M., Park, K. M., Reichert, R. J., Bell, P. D., Burdine, R. D. and Lipschutz, J. H. (2011). The exocyst protein Sec10 interacts with Polycystin-2 and knockdown causes PKD-phenotypes. *PLoS Genet.* **7**, e1001361.
Gangar, A., Rossi, G., Andreeva, A., Hales, R. and Brennwald, P. (2005). Structurally conserved interaction of Lgl family with SNAREs is critical to their cellular function. *Curr. Biol.* **15**, 1136-1142.
Gao, C., Wang, G., Amack, J. D. and Mitchell, D. R. (2010). Oda16/Wdr69 is essential for axonemal dynein assembly and ciliary motility during zebrafish embryogenesis. *Dev. Dyn.* **239**, 2190-2197.
Gateff, E. (1978). Malignant neoplasms of genetic origin in Drosophila melanogaster. *Science* **200**, 1448-1459.
Grosshans, B. L., Andreeva, A., Gangar, A., Niessen, S., Yates, J. R., 3rd, Brennwald, P. and Novick, P. (2006). The yeast lgl family member Sro7p is an effector of the secretory Rab GTPase Sec4p. *J. Cell Biol.* **172**, 55-66.
Haga, Y., Dominique, V. J., 3rd and Du, S. J. (2009). Analyzing notochord segmentation and intervertebral disc formation using the twhh:gfp transgenic zebrafish model. *Transgenic Res.* **18**, 669-683.
Hava, D., Forster, U., Matsuda, M., Cui, S., Link, B. A., Eichhorst, J., Wiesner, B., Chitnis, A. and Abdelilah-Seyfried, S. (2009). Apical membrane

maturation and cellular rosette formation during morphogenesis of the zebrafish lateral line. *J. Cell Sci.* **122**, 687-695.
Huang, C. J., Tu, C. T., Hsiao, C. D., Hsieh, F. J. and Tsai, H. J. (2003). Germ-line transmission of a myocardium-specific GFP transgene reveals critical regulatory elements in the cardiac myosin light chain 2 promoter of zebrafish. *Dev. Dyn.* **228**, 30-40.
Ishikawa, H. and Marshall, W. F. (2011). Ciliogenesis: building the cell's antenna. *Nat. Rev. Mol. Cell Biol.* **12**, 222-234.
Kane, D. A., McFarland, K. N. and Warga, R. M. (2005). Mutations in half baked/E-cadherin block cell behaviors that are necessary for teleost epiboly. *Development* **132**, 1105-1116.
Kaplan, N. A., Liu, X. and Tolwinski, N. S. (2009). Epithelial polarity: interactions between junctions and apical-basal machinery. *Genetics* **183**, 897-904.
Kimmel, C. B., Ballard, W. W., Kimmel, S. R., Ullmann, B. and Schilling, T. F. (1995). Stages of embryonic development of the zebrafish. *Dev. Dyn.* **203**, 253-310.
Klezovitch, O., Fernandez, T. E., Tapscott, S. J. and Vasioukhin, V. (2004). Loss of cell polarity causes severe brain dysplasia in Lgl1 knockout mice. *Genes Dev.* **18**, 559-571.
Knödler, A., Feng, S., Zhang, J., Zhang, X., Das, A., Peränen, J. and Guo, W. (2010). Coordination of Rab8 and Rab11 in primary ciliogenesis. *Proc. Natl. Acad. Sci. USA* **107**, 6346-6351.
Kramer-Zucker, A. G., Olale, F., Haycraft, C. J., Yoder, B. K., Schier, A. F. and Drummond, I. A. (2005). Cilia-driven fluid flow in the zebrafish pronephros, brain and Kupffer's vesicle is required for normal organogenesis. *Development* **132**, 1907-1921.
Krauss, S., Concordet, J. P. and Ingham, P. W. (1993). A functionally conserved homolog of the Drosophila segment polarity gene hh is expressed in tissues with polarizing activity in zebrafish embryos. *Cell* **75**, 1431-1444.
Lehman, K., Rossi, G., Adamo, J. E. and Brennwald, P. (1999). Yeast homologues of tomosyn and lethal giant larvae function in exocytosis and are associated with the plasma membrane SNARE, Sec9. *J. Cell Biol.* **146**, 125-140.
Lock, J. G. and Stow, J. L. (2005). Rab11 in recycling endosomes regulates the sorting and basolateral transport of E-cadherin. *Mol. Biol. Cell* **16**, 1744-1755.
Long, S., Ahmad, N. and Rebagliati, M. (2003). The zebrafish nodal-related gene southpaw is required for visceral and diencephalic left-right asymmetry. *Development* **130**, 2303-2316.
Matsui, T., Thitamadee, S., Murata, T., Kakinuma, H., Nabetani, T., Hirabayashi, Y., Hirate, Y., Okamoto, H. and Bessho, Y. (2011). Canopy1, a positive feedback regulator of FGF signaling, controls progenitor cell clustering during Kupffer's vesicle organogenesis. *Proc. Natl. Acad. Sci. USA* **108**, 9881-9886.
Melby, A. E., Warga, R. M. and Kimmel, C. B. (1996). Specification of cell fates at the dorsal margin of the zebrafish gastrula. *Development* **122**, 2225-2237.
Müsch, A., Cohen, D., Yeaman, C., Nelson, W. J., Rodriguez-Boulan, E. and Brennwald, P. J. (2002). Mammalian homolog of Drosophila tumor suppressor lethal (2) giant larvae interacts with basolateral exocytic machinery in Madin-Darby canine kidney cells. *Mol. Biol. Cell* **13**, 158-168.
Nonaka, S., Tanaka, Y., Okada, Y., Takeda, S., Harada, A., Kanai, Y., Kido, M. and Hirokawa, N. (1998). Randomization of left-right asymmetry due to loss of nodal cilia generating leftward flow of extraembryonic fluid in mice lacking KIF3B motor protein. *Cell* **95**, 829-837.
Okada, Y., Takeda, S., Tanaka, Y., Izpisúa Belmonte, J. C. and Hirokawa, N. (2005). Mechanism of nodal flow: a conserved symmetry breaking event in left-right axis determination. *Cell* **121**, 633-644.
Oteíza, P., Köppen, M., Concha, M. L. and Heisenberg, C. P. (2008). Origin and shaping of the laterality organ in zebrafish. *Development* **135**, 2807-2813.
Oteiza, P., Köppen, M., Krieg, M., Pulgar, E., Farias, C., Melo, C., Preibisch, S., Müller, D., Tada, M., Hartel, S. et al. (2010). Planar cell polarity signalling regulates cell adhesion properties in progenitors of the zebrafish laterality organ. *Development* **137**, 3459-3468.
Oztan, A., Silvis, M., Weisz, O. A., Bradbury, N. A., Hsu, S. C., Goldenring, J. R., Yeaman, C. and Apodaca, G. (2007). Exocyst requirement for endocytic traffic directed toward the apical and basolateral poles of polarized MDCK cells. *Mol. Biol. Cell* **18**, 3978-3992.
Plant, P. J., Fawcett, J. P., Lin, D. C., Holdorf, A. D., Binns, K., Kulkarni, S. and Pawson, T. (2003). A polarity complex of mPar-6 and atypical PKC binds, phosphorylates and regulates mammalian Lgl. *Nat. Cell Biol.* **5**, 301-308.
Rebagliati, M. R., Toyama, R., Fricke, C., Haffter, P. and Dawid, I. B. (1998). Zebrafish nodal-related genes are implicated in axial patterning and establishing left-right asymmetry. *Dev. Biol.* **199**, 261-272.
Reischauer, S., Levesque, M. P., Nüsslein-Volhard, C. and Sonawane, M. (2009). Lgl2 executes its function as a tumor suppressor by regulating ErbB signaling in the zebrafish epidermis. *PLoS Genet.* **5**, e1000720.
Robu, M. E., Larson, J. D., Nasevicius, A., Beiraghi, S., Brenner, C., Farber, S. A. and Ekker, S. C. (2007). p53 activation by knockdown technologies. *PLoS Genet.* **3**, e78.
Rodríguez-Fraticelli, A. E., Gálvez-Santisteban, M. and Martín-Belmonte, F. (2011). Divide and polarize: recent advances in the molecular mechanism regulating epithelial tubulogenesis. *Curr. Opin. Cell Biol.* **23**, 638-646.
Sakaguchi, T., Kikuchi, Y., Kuroiwa, A., Takeda, H. and Stainier, D. Y. (2006). The yolk syncytial layer regulates myocardial migration by influencing extracellular matrix assembly in zebrafish. *Development* **133**, 4063-4072.
Schweickert, A., Weber, T., Beyer, T., Vick, P., Bogusch, S., Feistel, K. and Blum, M. (2007). Cilia-driven leftward flow determines laterality in Xenopus. *Curr. Biol.* **17**, 60-66.
Sharma, N., Berbari, N. F. and Yoder, B. K. (2008). Ciliary dysfunction in developmental abnormalities and diseases. *Curr. Top. Dev. Biol.* **85**, 371-427.
Shewan, A. M., Maddugoda, M., Kraemer, A., Stehbens, S. J., Verma, S., Kovacs, E. M. and Yap, A. S. (2005). Myosin 2 is a key Rho kinase target necessary for the local concentration of E-cadherin at cell-cell contacts. *Mol. Biol. Cell* **16**, 4531-4542.
Smutny, M., Cox, H. L., Leerberg, J. M., Kovacs, E. M., Conti, M. A., Ferguson, C., Hamilton, N. A., Parton, R. G., Adelstein, R. S. and Yap, A. S. (2010). Myosin II isoforms identify distinct functional modules that support integrity of the epithelial zonula adherens. *Nat. Cell Biol.* **12**, 696-702.
Sonawane, M., Carpio, Y., Geisler, R., Schwarz, H., Maischein, H. M. and Nuesslein-Volhard, C. (2005). Zebrafish penner/lethal giant larvae 2 functions in hemidesmosome formation, maintenance of cellular morphology and growth regulation in the developing basal epidermis. *Development* **132**, 3255-3265.
Sonawane, M., Martin-Maischein, H., Schwarz, H. and Nüsslein-Volhard, C. (2009). Lgl2 and E-cadherin act antagonistically to regulate hemidesmosome formation during epidermal development in zebrafish. *Development* **136**, 1231-1240.
Sripathy, S., Lee, M. and Vasioukhin, V. (2011). Mammalian Llgl2 is necessary for proper branching morphogenesis during placental development. *Mol. Cell. Biol.* **31**, 2920-2933.
Stenmark, H. (2009). Rab GTPases as coordinators of vesicle traffic. *Nat. Rev. Mol. Cell Biol.* **10**, 513-525.
Strand, D., Jakobs, R., Merdes, G., Neumann, B., Kalmes, A., Heid, H. W., Husmann, I. and Mechler, B. M. (1994). The Drosophila lethal(2)giant larvae tumor suppressor protein forms homo-oligomers and is associated with nonmuscle myosin II heavy chain. *J. Cell Biol.* **127**, 1361-1373.
Tanentzapf, G. and Tepass, U. (2003). Interactions between the crumbs, lethal giant larvae and bazooka pathways in epithelial polarization. *Nat. Cell Biol.* **5**, 46-52.
Wan, Q., Liu, J., Zheng, Z., Zhu, H., Chu, X., Dong, Z., Huang, S. and Du, Q. (2012). Regulation of myosin activation during cell-cell contact formation by Par3-Lgl antagonism -entosis without matrix detachment. *Mol. Biol. Cell* **23**, 2076-2091.
Wang, G., Cadwallader, A. B., Jang, D. S., Tsang, M., Yost, H. J. and Amack, J. D. (2011a). The Rho kinase Rock2b establishes anteroposterior asymmetry of the ciliated Kupffer's vesicle in zebrafish. *Development* **138**, 45-54.
Wang, T., Liu, Y., Xu, X. H., Deng, C. Y., Wu, K. Y., Zhu, J., Fu, X. Q., He, M. and Luo, Z. G. (2011b). Lgl1 activation of rab10 promotes axonal membrane trafficking underlying neuronal polarization. *Dev. Cell* **21**, 431-444.
Westlake, C. J., Baye, L. M., Nachury, M. V., Wright, K. J., Ervin, K. E., Phu, L., Chalouni, C., Beck, J. S., Kirkpatrick, D. S., Slusarski, D. C. et al. (2011). Primary cilia membrane assembly is initiated by Rab11 and transport protein particle II (TRAPPII) complex-dependent trafficking of Rabin8 to the centrosome. *Proc. Natl. Acad. Sci. USA* **108**, 2759-2764.
Yu, X., Lau, D., Ng, C. P. and Roy, S. (2011). Cilia-driven fluid flow as an epigenetic cue for otolith biomineralization on sensory hair cells of the inner ear. *Development* **138**, 487-494.
Zhang, X., Wang, P., Gangar, A., Zhang, J., Brennwald, P., TerBush, D. and Guo, W. (2005). Lethal giant larvae proteins interact with the exocyst complex and are involved in polarized exocytosis. *J. Cell Biol.* **170**, 273-283.

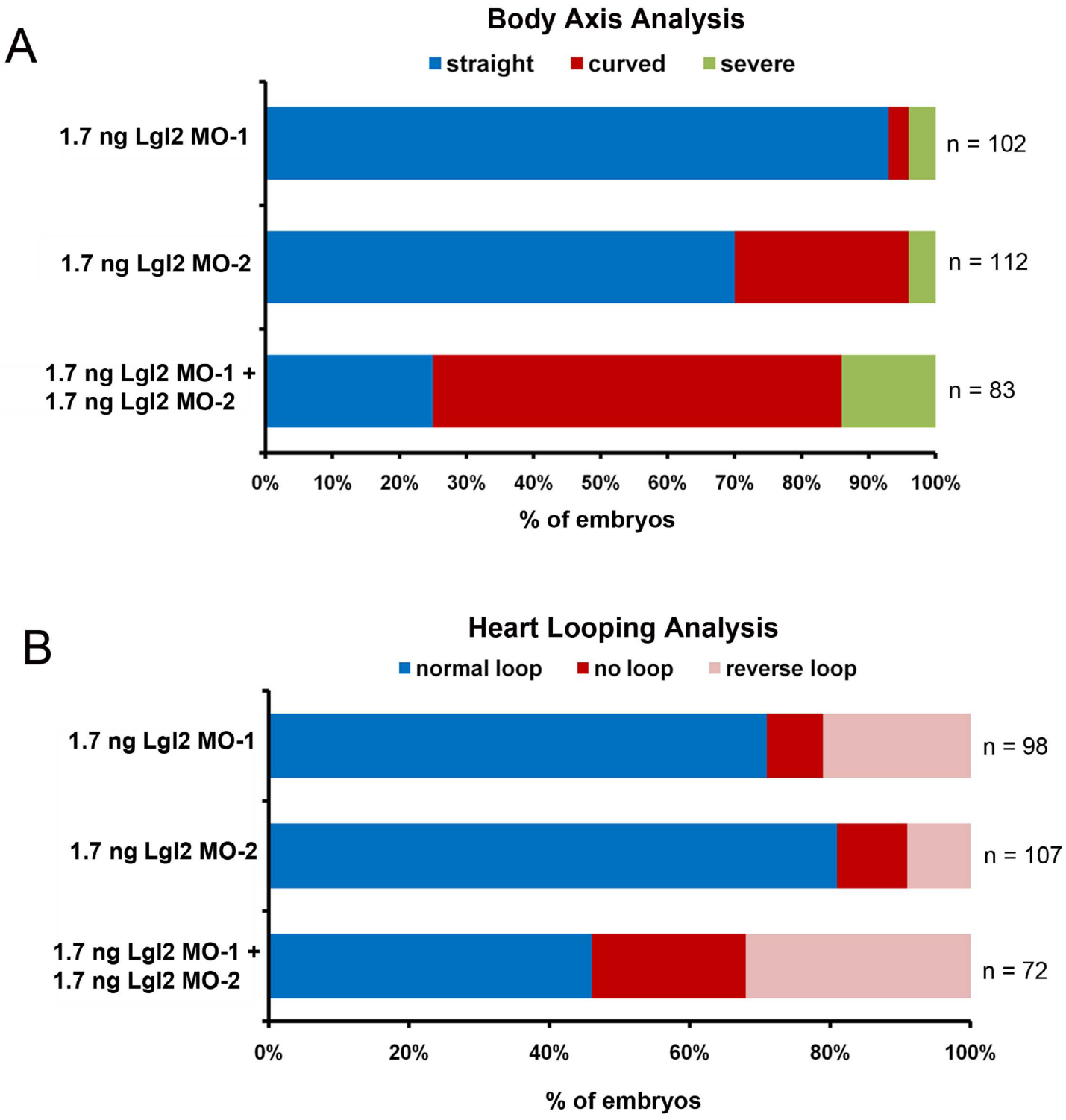

Fig. S1. Co-injection of sub-optimal doses of two different Lgl2 MOs recapitulated Lgl2 knockdown phenotypes. Analysis of embryos injected with a sub-optimal dose (1.7 ng) of Lgl2 MO-1, a sub-optimal dose of Lgl2 MO-2 (1.7 ng) or co-injected with both. (**A**) Percentage of embryos with body axis defects at 48 hpf. (**B**) Percentage of embryos with heart-looping defects at 48 hpf. *n*, number of embryos analyzed.

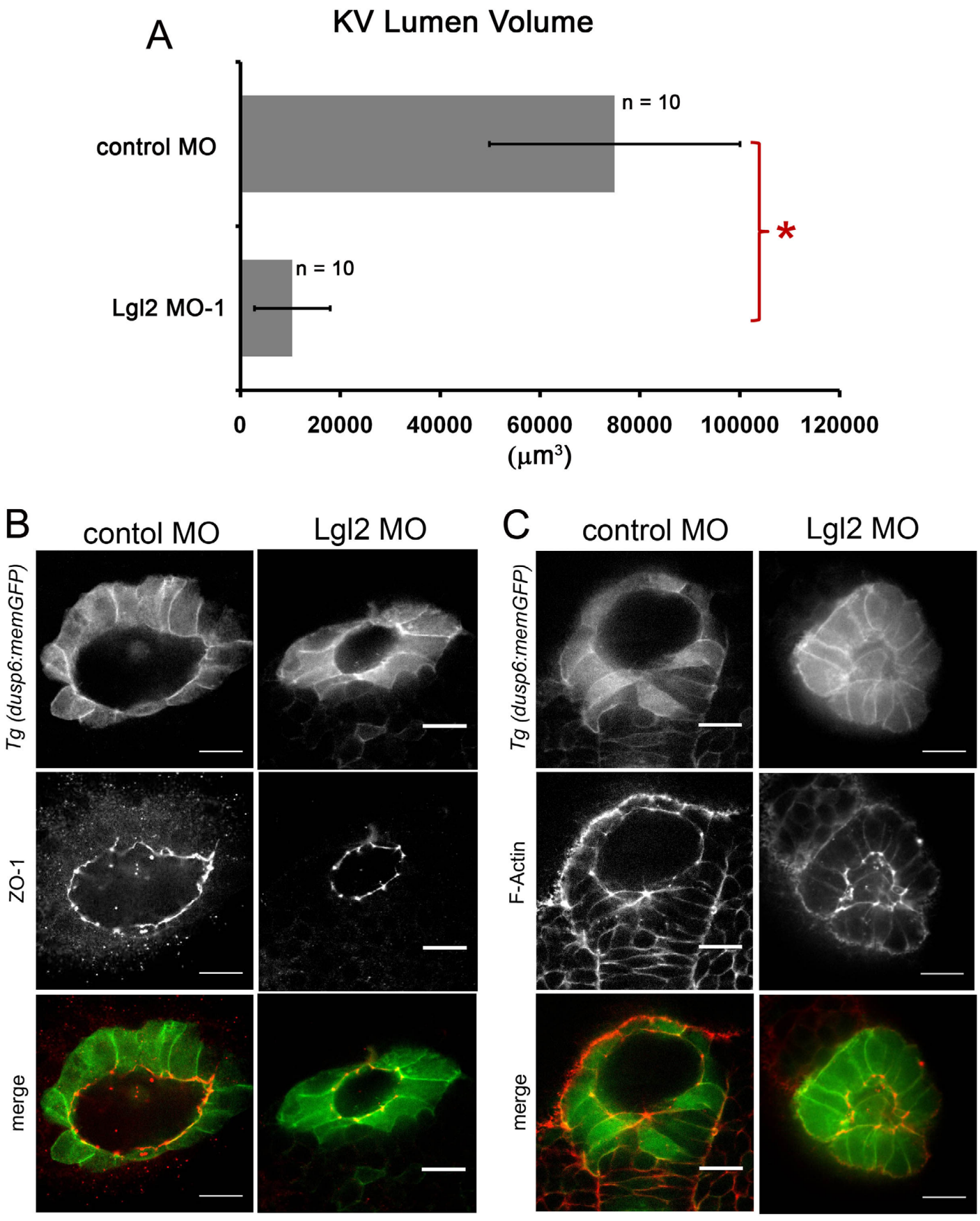

Fig. S2. Depletion of Lgl2 reduced KV lumen volume, but did not alter localization of apical epithelial markers. (**A**) Analysis of KV lumen volume at the 8-somite stage in live *Tg(dusp6:memGFP)* embryos. Error bars represent s.d. *n*, number of embryos analyzed. **P*<0.05. (**B**,**C**) Fluorescence staining of apical markers in *Tg(dusp6:memGFP)* embryos injected with control MO or Lgl2 MO. ZO-1 (B) and F-Actin (C) were localized at apical membranes lining the KV lumen in both control and Lgl2-depleted embryos. Scale bars: 20 μm.

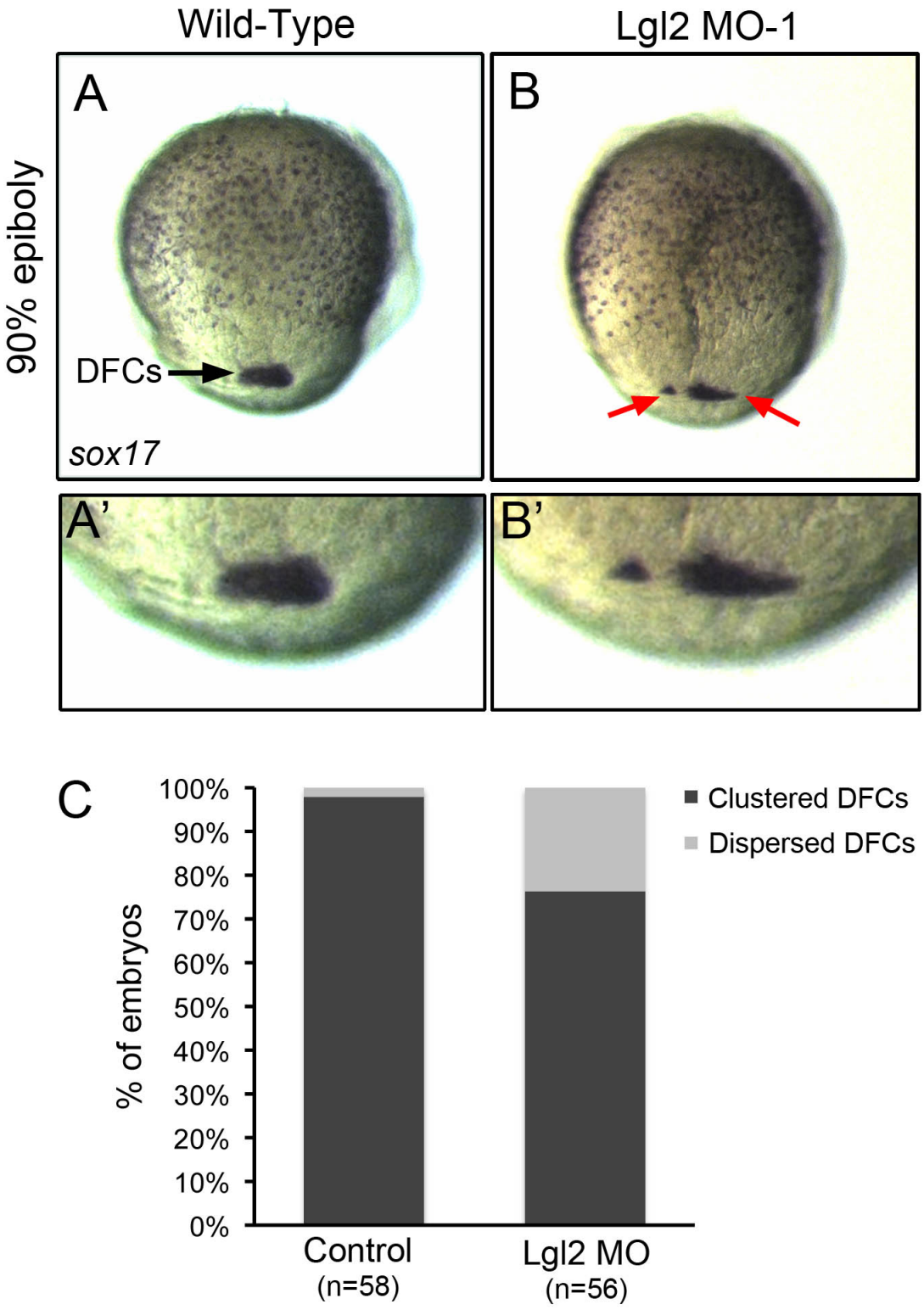

Fig. S3. DFC clustering was disrupted in a subset of Lgl2 knockdown embryos. (**A-B**′) RNA *in situ* hybridization of *sox17* expression was used to analyze DFCs (arrows) at the 90% epiboly stage. A′ and B′ are magnified views of DFCs in A and B, respectively. (**C**) DFCs were tightly clustered in most control embryos (A,A′C), whereas DFCs were dispersed in 23% of Lgl2 MO embryos (B,B′,C). *n*, number of embryos analyzed.

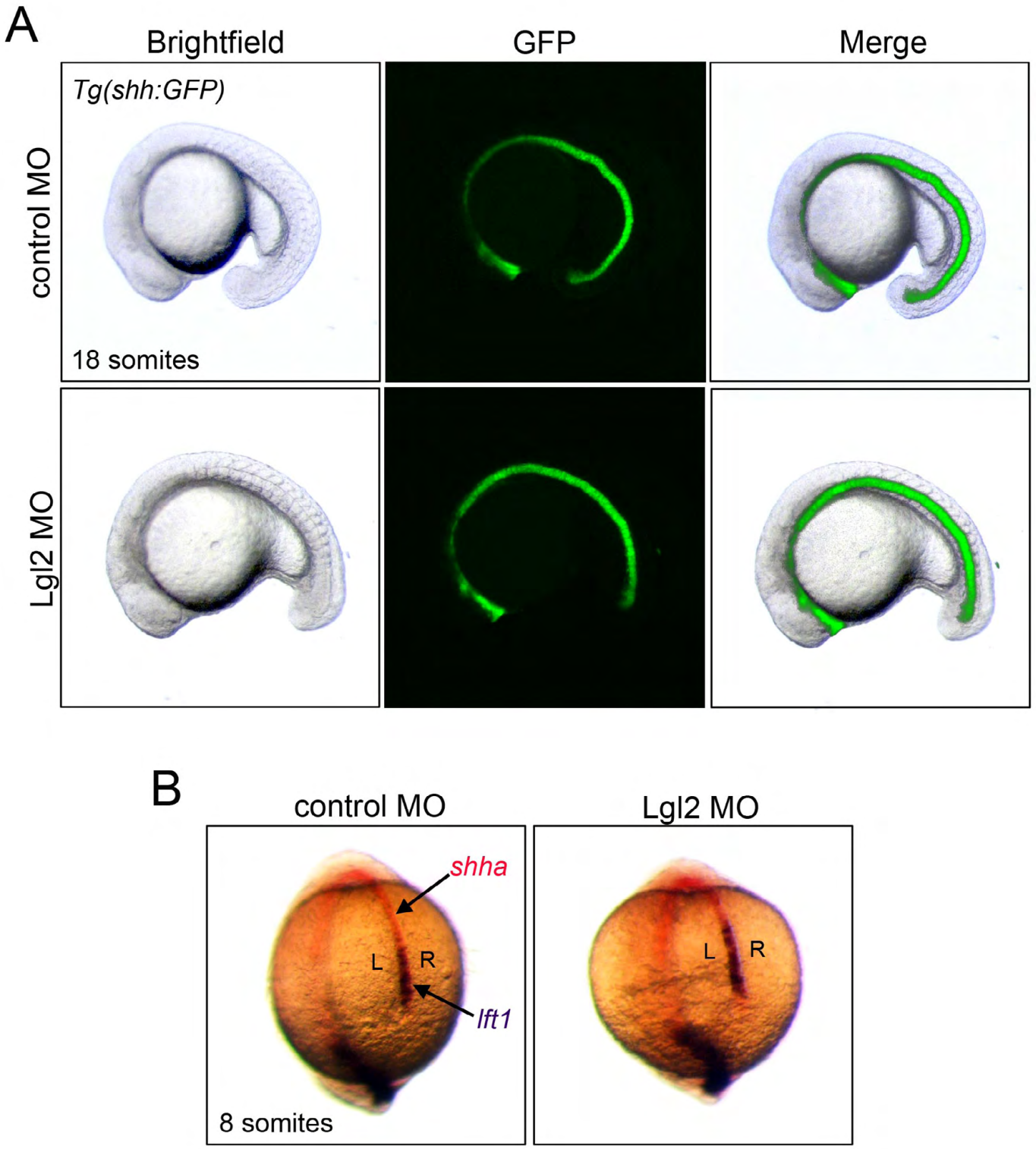

Fig. S4. The embryonic midline is intact in Lgl2-depleted embryos. (**A**) Lateral views of live *Tg(shh:GFP)* embryos that express GFP in the notochord. The notochord was intact and appeared similar in control MO and Lgl2 MO embryos at the 18-somite stage. (**B**) Posterior views of double RNA *in situ* hybridization staining of *sonic hedgehog* (*shha*; red) and *lefty1* (*lft1*; purple) at the 8-somite stage when *lft1* expression is initiated in the posterior notochord. Strong *lft1* expression in the notochord, which provides a molecular barrier between left (L) and right (R), was observed in most control MO (83%, *n*=72) and Lgl2 MO (84%, *n*=56) embryos, indicating *lft1* activation is not delayed in Lgl2 MO embryos.

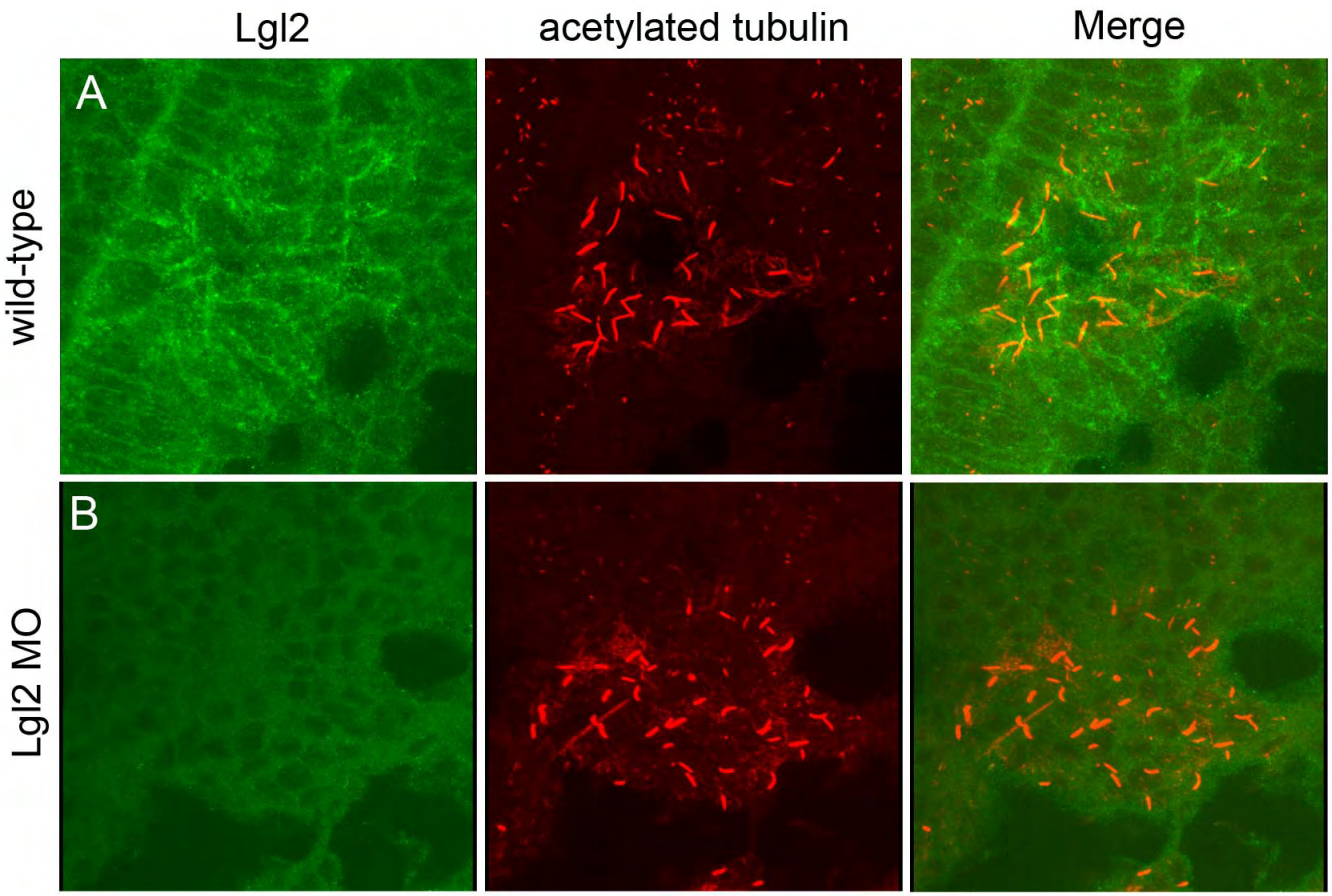

Fig. S5. Lgl2 antibody staining is reduced in Lgl2 MO embryos. (**A**,**B**) Maximum projections of Lgl2 and acetylated tubulin immunostaining in the KV region show that the membrane-localized Lgl2 staining observed in the uninjected embryos (A) is reduced in Lgl2 MO embryos (B).

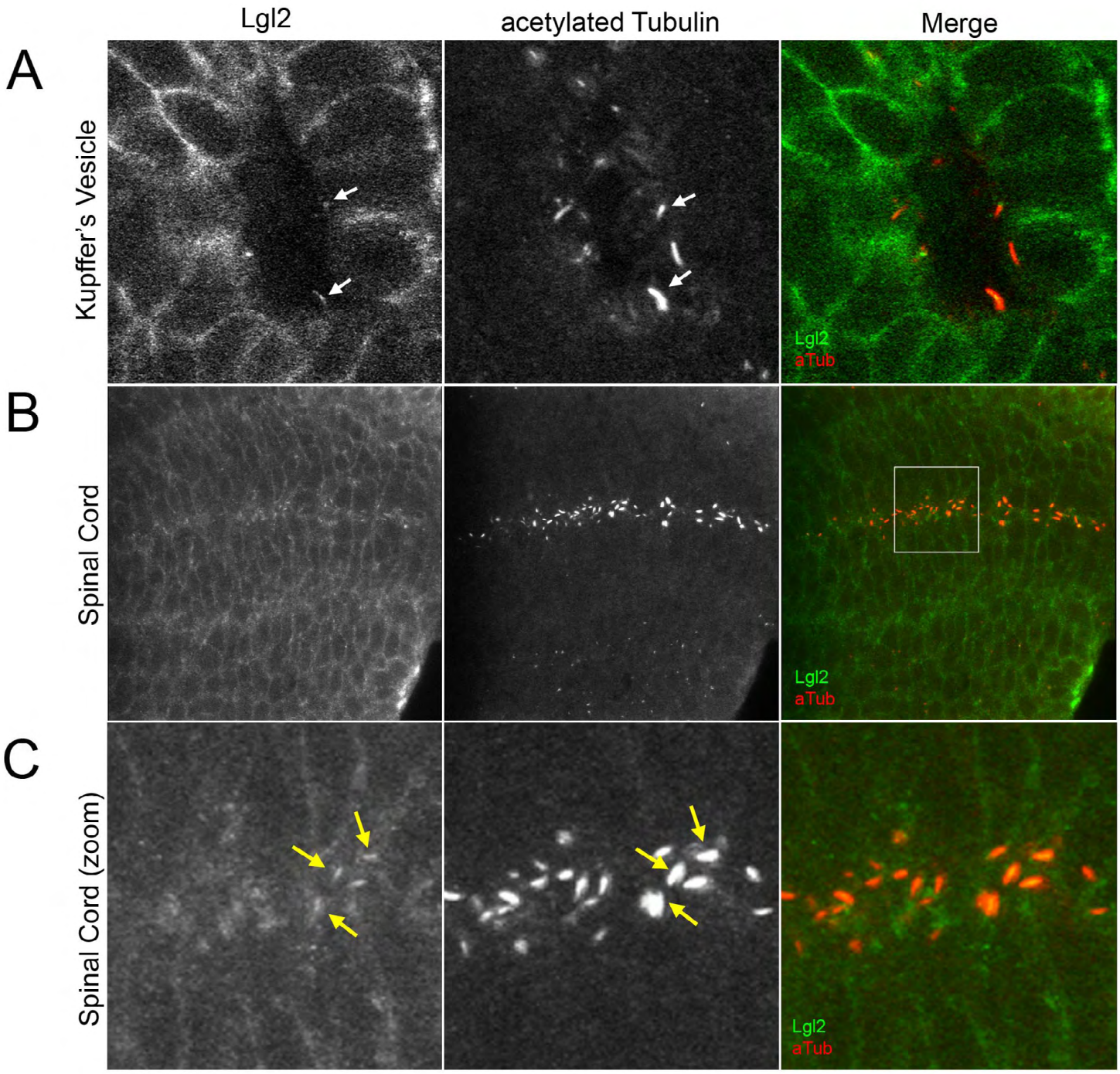

Fig. S6. Lgl2 localizes to cell membranes and some motile cilia in KV and the spinal cord. (**A-C**) Whole embryo fluorescence immunostaining using Lgl2 antibodies and acetylated tubulin antibodies indicates that Lgl2 localizes to cell membranes and colocalizes with acetylated tubulin in in some KV cilia (arrows in A) and cilia in the spinal cord (arrows in B,C) in wild-type embryos. The box in B identifies the region enlarged in C.

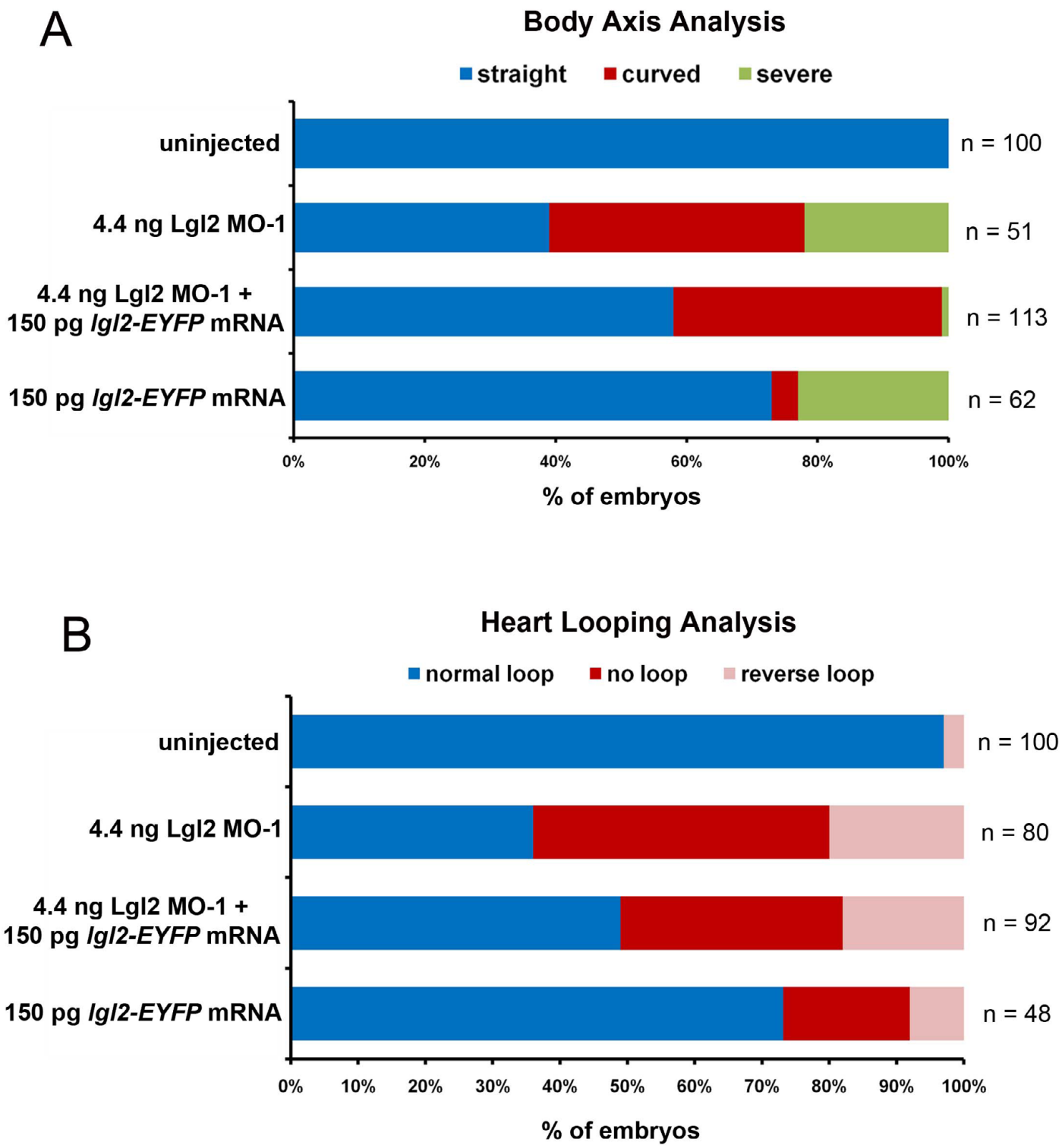

Fig. S7. Lgl2:EYFP fusion protein partially rescues Lgl2 MO phenotypes. (**A**,**B**) Percentage of uninjected control embryos and embryos injected with Lgl2 MO, Lgl2 MO + mRNA encoding *Lgl2:EYFP,* or *Lgl2:EYFP* mRNA alone with body axis defects (A) and heart-looping defects (B) at 48 hpf. *n*, number of embryos analyzed.

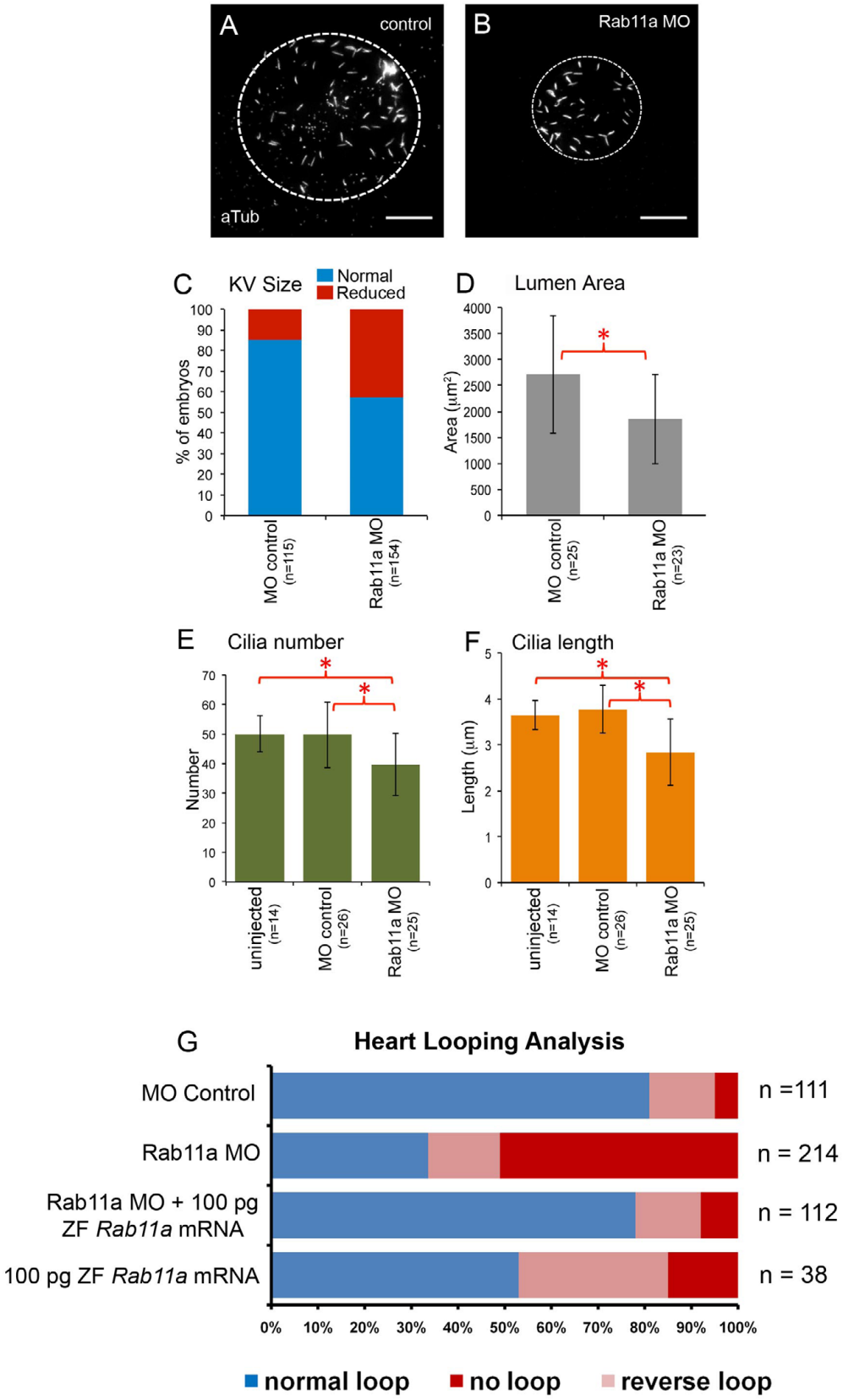

Fig. S8. Rab11a MO knockdown disrupted KV development and left-right asymmetry. (**A**,**B**) KV cilia immunostained with acetylated tubulin antibodies showing a reduced KV size concomitant with a slight reduction in cilia number and length in embryos injected with an optimal dose of Rab11a MO (B) relative to MO control (A). The dashed circle outlines the approximate boundary of KV lumen. Scale bars: 20 μm. (**C**) Approximately 43% of the Rab11a MO embryos contained a reduced KV compared with MO control embryos. (**D**) Quantification of KV lumen area. (**E**,**F**) KV cilia number (E) and length (F) were significantly reduced in Rab11a MO embryos relative to controls. Error bars represent s.d. *n*, number of embryos analyzed. **P*<0.05. (**G**) Consistent with KV defects, embryos injected with an optimal dose of Rab11a MO showed defects in heart left-right asymmetry. These defects were partially rescued by co-injecting *rab11a* mRNA. *n*, number of embryos analyzed.

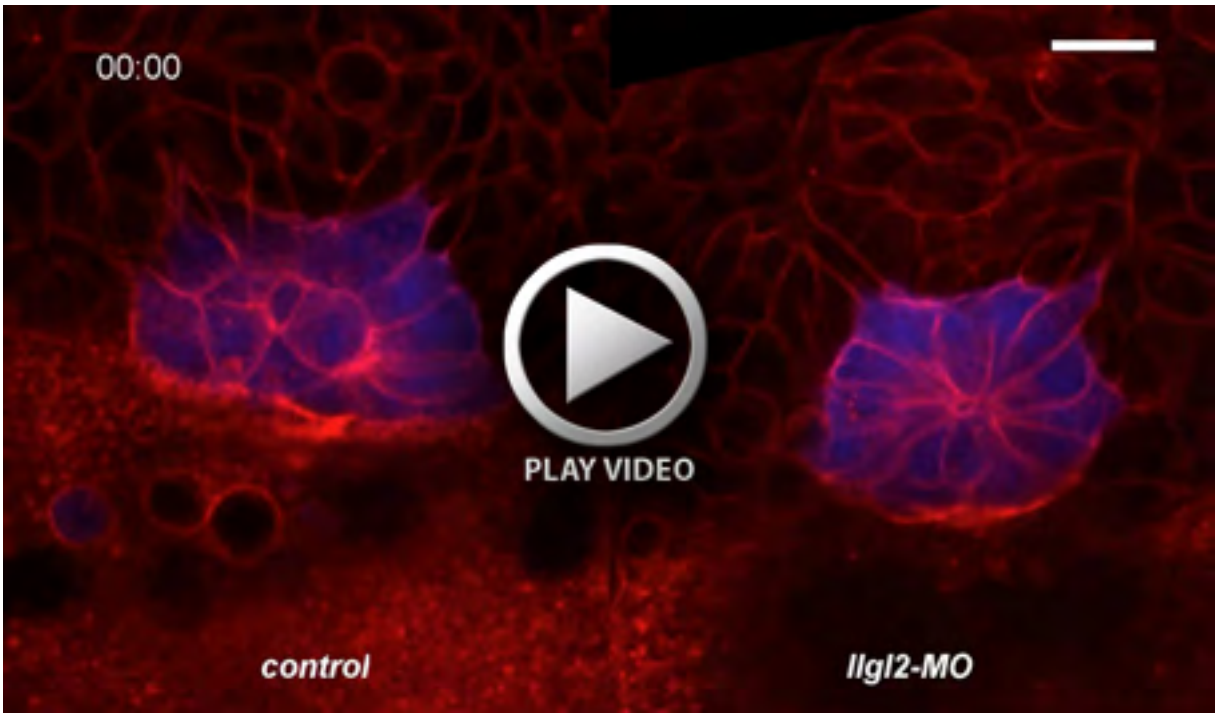

Movie 1. Time-lapse imaging of KV morphogenesis in double transgenic *Tg(sox17:GFP;* β*-actin:Lyn-TdTomato)* embryos in which GFP (pseudocolored blue) labels KV cells and TdTomato (red) marks plasma membranes. Images were captured every 450 seconds between the 1-somite stage and the 5-somite stage of development. Lumen expansion proceeded normally in the uninjected control embryo, whereas lumen development was disrupted in the Lgl2 MO-injected embryo.

Model 1. Full model with secreted Wnt inhibitor (Inh) and with Wnt signalling regulating Inh gene expression both via cardiogenic transcription factor genes and more directly (see Fig. 8A). Simulation predicts most reliable and reproducible patterning (see Fig. 8B-D). BioTapestry files and Dizzy-compatible SBML files are provided here and for each model.

Download Model 1.

Model 2. Full model with secreted Wnt inhibitor (Inh) as in Model 1 but with Wnt signalling regulating Inh gene expression only via cardiogenic transcription factor genes. Simulation predicts fairly reliable and reproducible patterning (see Fig. 8E).

Download Model 2.

Model 3. As in Model 1 but without Inh gene expression (mimicking sfrp1MO experiment, see Fig. 3P,R). Simulation predicts reduced myocardium differentiation (see Fig. 8F,G).

Download Model 3.

Model 4. As in Model 1 but without Wnt (and without Inh gene expression, mimicking sfrp1MO wnt6MO3 double knockdown experiment, see Fig. 7M). Simulation predicts dramatically increased myocardium differentiation (see Fig. 8H,I).

Download Model 4.

Model 5. Full model with Wnt signal and with endogenous secreted Wnt inhibitor (Inh) as in Model 1 but additionally with a transgene providing a pulse of Inh expression at the beginning of the simulation period (mimicking the stage-specific sfrp1 overexpression experiment, see Fig. 4R,T). Simulation predicts dramatically increased myocardium differentiation (see Fig. 8H,I).

Download Model 5.

Model 6. Full model with Wnt signal and with endogenous secreted Wnt inhibitor (Inh) as in Model 1 but without Wnt signalling regulating Inh gene expression. Simulation predicts intermediate state (meaning confused cell identity) of some cells and therefore no clear patterning into peri- and myocardium (predictably, this model resembles Model 7 below). Comparing the simulation of this model with the simulation of models 1, 2 and 9 suggests that the negative regulation of Inh gene expression is an important and fundamental aspect of the GRN regulating heart muscle differentiation.

Download Model 6.

Model 7. An alternative model with only Wnt signalling patterning myocardium development (i.e without any Inh gene), which differs from Model 3 in that Wnt signalling was adjusted to result mostly in at least two cells differentiating as myocardium and two cells as pericardium. Simulation predicts intermediate state (meaning confused cell identity) of some cells and therefore no clear patterning into peri- and myocardium (see Fig. 8J,K).

Download Model 7.

Model 8. An alternative model with only Wnt signalling patterning myocardium development (i.e without any Inh gene) and therefore similar to Model 7, but assuming a higher order of cooperativity in the autoregulation of cardiogenic transcription factor genes. Simulation predicts reliable clear patterning into either peri- or myocardium cell differentiation, but compared with Model 1 with a less reproducible patterning into two peri- and four myocardium cells (an outcome similar to Model 9 below).

Download Model 8.

Model 9. An alternative model similar to Model 1 but with a cell-autonomous Wnt inhibitor (Inh), but still with Wnt signalling regulating Inh gene expression both via cardiogenic transcription factor genes and more directly with only Wnt signalling patterning myocardium development. Simulation predicts reliable clear patterning into either peri- or myocardium cell differentiation, but compared with Model 1 with a less reproducible patterning into two peri- and four myocardium cells (see Fig. 8L,M).

Download Model 9.

Table S1. Asymmetric expression of LR markers is altered in Lgl2 MO embryos.

***pitx2c* Expression**

Embryos	Left	Right	Bilateral	Absent	*n*
Wild type	81%	0%	9.5%	9.5%	127
Lgl2 MO-2	37%	3%	30%	30%	163
Lgl2 MO-2 + lgl2 mRNA	48%	12%	25%	15%	67

***cyc* Expression**

Embryos	Left	Right	Bilateral	Absent	*n*
Wild type	73%	0%	12%	15%	*99*
Lgl2 MO-2	25%	7%	38%	30%	*73*
Lgl2 MO-2+ *lgl2* mRNA	31.5%	3%	40.5%	25%	*89*